The Wiener-Hopf solution of the isotropic penetrable wedge problem: diffraction and total field

The Wiener-Hopf solution of the isotropic penetrable wedge problem: diffraction and total field

Vito Daniele, and Guido Lombardi, *Member, IEEE*

***Abstract*— The diffraction of an incident plane wave by an isotropic penetrable wedge is studied using generalized Wiener-Hopf equations, and the solution is obtained using analytical and numerical-analytical approaches that reduce the Wiener-Hopf factorization to Fredholm integral equations of second kind. Mathematical aspects are described in a unified and consistent theory for angular region problems. The formulation is presented in the general case of skew incidence and several numerical tests at normal incidence are reported to validate the new technique.**

The solutions consider engineering applications in terms of GTD/UTD diffraction coefficients and total fields.

***Index Terms*— Wedges, Isotropic media, Wiener-Hopf method, Spectral factorization, Fredholm integral equations, Analytical-numerical methods, Geometrical optics, Electromagnetic diffraction, Geometrical and Uniform theory of diffraction.**

I. Introduction

Nowadays, accurate and efficient solutions of diffraction problems are of great interest in engineering, mathematical and physical communities.

This paper presents a general solution of the diffraction by an isotropic penetrable wedge, see Fig. 1. The diffraction by a penetrable wedge has constituted in the last century and constitutes an important and challenging problem. Several attempts to find the solution have been reported in literature [1]-[31], where different formulations and analytical and/or numerical approaches have been presented. All the cited papers are of great interest, however some of them proposed incorrect methods and/or solutions.

One of the most interesting attempts to solve the penetrable wedge problem was proposed in 1964 by Radlow [1]. This author provided a solution for the diffraction by the right-angled dielectric wedge solving a multidimensional Wiener-Hopf equation. In 1969, Kraut et al. ascertained that this solution was wrong [3]. Moreover the methods proposed by Zavadskii [2], and Aleksandrova-Khiznyak [5] were also wrong, see [7].

In 1977 Rawlins [8] provided a solution of the dielectric wedge problem using a general Integral Equation formulation, which is based on a standard perturbation technique. Its method was generalized in 1991 by Kim et al. These authors proposed an approximate solution of an arbitrary-angled dielectric wedge, which is obtained by performing physical optic approximation to the dual integral equation in the spatial frequency domain [12]-[13]: the results are presented in terms of diffraction coefficients and far-field patterns.

Manuscript received —; revised —.

The authors are with the Dipartimento di Elettronica, Politecnico di Torino, Corso Duca degli Abruzzi 24, 10129 Torino, Italy (emails: vito.daniele@polito.it, guido.lombardi@polito.it, fax: +39-011-5644099).

Vito Daniele is also with Istituto Superiore Mario Boella (ISMB), Torino, Italy, (web: http://www.ismb.it/).

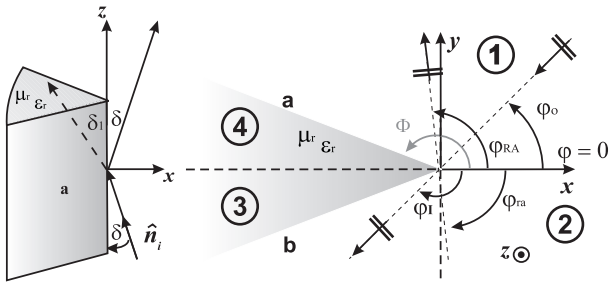

Fig. 1. The isotropic penetrable wedge.

In 1995 Budaev proposed the application of the popular and effective technique known as Sommerfeld-Malyuzhinets (SM) method (for instance see [19] and [32]), to deal with dielectric wedge problems [18]. The difference equations that arise from this formulation are originally reduced to singular integral equations. A regularization method reduces them to Fredholm equations. Budaev focused his monograph on the correct mathematical formulations avoiding engineering speculations such as the evaluation of the diffraction coefficients.

In the authors' opinion, the most significant results obtained for the penetrable wedge geometries arise from works using formulations in the one-dimensional spectral domain as in [18]. Some of these works produced very important contributions. In particular, in 1999, the monograph about elastic wedge by Croisille and Lebeau [21] presents a formulation of the problem in terms of singular integral equations in the Fourier domain: these equations were successfully solved by using the Galerkin collocation method. Theoretical and numerical aspects of Budaev's work were discussed in several papers, see for example [22] and references therein. In particular the paper by Kamotski et al. [22] has investigated the diffraction phenomena in an elastic wedge.

Formulations in a one-dimensional spectral domain based on the Kontorovich-Lebedev (KL) transform have been proposed in [9] and [15]. In particular, in 2006, Salem et al. estimate the electromagnetic field excited by a line source in the presence of an infinite dielectric wedge [29]: the solution is given in terms of asymptotic approximations for the near and far fields inside and outside the dielectric wedge.

In this paper we present a new method in the one-dimensional spectral domain based on the Wiener-Hopf (WH) technique. It constitutes an extension of the Wiener-Hopf formulation for impenetrable wedge problems that has been exhaustively considered in the past by Daniele and Lombardi [33]-[36]. The central problem of the proposed method is the factorization of matrix kernels in the WH formulation. Even though this problem has been considerably studied in the past, a general method to analytically factorize an arbitrary

matrix is not known up to now. Since the isotropic penetrable wedge with arbitrary aperture angle is a problem where no closed-form general WH factorization is available, we propose optimal approximate factorizations by using the Fredholm method introduced in [37] and [34] (inspired by [38]) that reduces the factorization problem to the solution of Fredholm integral equations of second kind.

For the sake of simplicity, in this work, we first present the WH formulation of the isotropic penetrable wedge's diffraction problem of a plane wave at skew incidence, and then we solve the diffraction by a dielectric wedge at normal incidence focusing the paper on all the mathematical/physical properties to get the solution. This paper is organized as follows: Section II deduces the Generalized Wiener-Hopf Equations (GWHE) of the isotropic penetrable wedge at skew incidence. After introducing useful mappings, the GWHE are reduced to two systems of equations with classical WH unknowns. These Classical Wiener-Hopf Equations (CWHE) are solved using the Fredholm factorization method [37] that reduces the factorization problem to the solution of systems of Fredholm integral equations of second kind. Section III shows the numerical implementation of the proposed method for the case of an E-polarized plane wave incident on a dielectric wedge. In particular we present the numerical solution of the Fredholm equations for the normal incident case and we provide approximate representations of an analytical element of the WH unknowns in the angular complex plane w. The same section addresses the analytical continuation of the approximate representations. Section IV deals with the evaluation of the electromagnetic far-field in the whole spatial domain for the normal incident case. In particular this section presents the solution in term of total field by estimating the field components: the Geometrical Optics (GO) component, the diffracted component, possible surface and lateral waves. Note that the geometrical optics contribution can be deduced from the WH formulation without the necessity of solving the Fredholm equations. Finally, numerous significant test cases are presented in section V to validate our technique and practical discussions are included. We conclude the paper with three Appendices which are fundamental from an implementation point of view. The first is devoted to the evaluation of the source term in the Fredholm equation in the case of a plane wave incident to the wedge. The second Appendix concerns the special mappings used in the analytical continuation of the approximate solutions, and the third one is focused on spectral properties of the solution. For the sake of brevity, we have omitted several mathematical proofs that the reader can find in [28], [35], [37], [41]- [42]. We assert that an important advantage of using the GWHE formulation (as well as the spectral method proposed in [21]) is the possibility to solve wedge problems immersed in anisotropic or bianisotropic media. Apparently this extension is not possible in the framework of the Sommerfeld-Malyuzhinets formulations.

II. The Wiener-Hopf formulation

Fig. 1 illustrates the problem of the diffraction of a plane wave at skew incidence by an isotropic penetrable wedge having permittivity $\varepsilon_1 = \varepsilon_o\varepsilon_r$ and permeability $\mu_1 = \mu_o\mu_r$ immersed in the free space (permittivity ε_o and permeability μ_o). We consider the cylindrical coordinate system (ρ, φ, z) and time harmonic electromagnetic fields with a time dependence specified by the factor $e^{j\omega t}$ which is omitted. The incident field is constituted by plane waves having the following longitudinal components:

$$\left\{\begin{array}{lcl} E_z^i &=& E_o e^{j\tau_o \rho\cos(\varphi-\varphi_o)} e^{-j\gamma_o z} \\ H_z^i &=& H_o e^{j\tau_o \rho\cos(\varphi-\varphi_o)} e^{-j\gamma_o z} \end{array}\right. \tag{1}$$

where: δ and φ_o ($\varphi_I = \varphi_o - \pi$) are respectively the zenithal and the azimuthal angles which define the direction of the plane wave, $k_o = \omega\sqrt{\mu_o\,\varepsilon_o}$ is the wave number and, $\gamma_o = k_o\cos\delta$ and $\tau_o = k_o\sin\delta$ are respectively the longitudinal component and the transverse component of the wave vector.

Fig. 1 shows two media and four angular regions: 1) $0 < \varphi < \Phi$, 2) $-\Phi < \varphi < 0$, 3) $-\pi < \varphi < -\Phi$, and 4) $\Phi < \varphi < \pi$. The first two regions are in free space, the second two are in the isotropic penetrable medium that constitutes the wedge. To facilitate the readability of the paper, we will extensively use the supplementary angles $\varphi_1 = \pi - \varphi$ and $\Phi_1 = \pi - \Phi$ for the definition of quantities inside the wedge. According to geometrical optics, the field inside the isotropic penetrable medium is characterized by: the wave number $k_1 = \omega\sqrt{\mu_o\mu_r\varepsilon_o\varepsilon_r}$, the longitudinal component and the transverse component of the wave vector $\gamma_1 = k_1\cos\delta_1$ and $\tau_1 = k_1\sin\delta_1$ where δ_1 is determined by enforcing $\gamma_1 = \gamma_o$ (the electromagnetic properties of the wedge are independent of z).

The Wiener-Hopf technique for angular regions' problems [33], [35] is based on the Laplace transforms of the longitudinal and tangential components of the electromagnetic field:

$$\begin{array}{lcl} V_{z+}(\eta,\varphi) &=& \int_0^\infty E_z(\rho,\varphi)e^{j\eta\rho}d\rho, \\ I_{z+}(\eta,\varphi) &=& \int_0^\infty H_z(\rho,\varphi)e^{j\eta\rho}d\rho \\ V_{\rho+}(\eta,\varphi) &=& \int_0^\infty E_\rho(\rho,\varphi)e^{j\eta\rho}d\rho, \\ I_{\rho+}(\eta,\varphi) &=& \int_0^\infty H_\rho(\rho,\varphi)e^{j\eta\rho}d\rho \end{array} \tag{2}$$

where the subscript $+$ $(-)$ indicates plus (minus) functions, *i.e.* functions whose regular half-plane is the upper (lower) half η-plane. To avoid the presence of singularities on the real axis, we assume k_o with a small negative imaginary part. In the following we will use multiple complex planes (η plane and $-m$ plane) for the definition of Laplace transforms along different directions φ:

$$\begin{array}{ll} F_+(\eta,0) & = \int_0^\infty f(\rho,0)e^{j\eta\rho}d\rho, \\ F_+(-m,\pm\Phi) & = \int_0^\infty f(\rho,\pm\Phi)e^{-jm\rho}d\rho \end{array} \tag{3}$$

According to the theory presented in [28], [33], [35], [39]-[42] the generalized Wiener-Hopf equations for the diffraction of a plane wave at skew incidence by a penetrable wedge are reported in (4), (5), (6), and (7) respectively for the angular regions of Fig. 1 numbered in ascending order. The GWHE are written in terms of the following quantities (8). Note that, in the expression $\xi = \sqrt{\tau_o^2 - \eta^2}$ ($\xi_1 = \sqrt{\tau_1^2 - \eta^2}$) we define the proper branch of the square root the one that assumes the value τ_o (τ_1) for $\eta = 0$.

$$\left\{\begin{array}{l} \xi = \sqrt{\tau_o^2 - \eta^2}; \quad \xi_1 = \sqrt{\tau_1^2 - \eta^2} \\ m = -\eta\cos\Phi + \xi\sin\Phi \\ m_1 = -\eta\cos\Phi_1 + \xi_1\sin\Phi_1 \\ n = -\eta\sin\Phi - \xi\cos\Phi \\ n_1 = -\eta\sin\Phi_1 - \xi_1\cos\Phi_1 \end{array}\right. \tag{8}$$

$$\begin{cases} \xi\, V_{z+}(\eta,0) - \frac{\tau_o^2}{\omega\,\varepsilon_o} I_{\rho+}(\eta,0) - \frac{\gamma_o\,\eta}{\omega\,\varepsilon_o} I_{z+}(\eta,0) = -n\ V_{z+}(-m,\Phi) - \frac{\tau_o^2}{\omega\,\varepsilon_o} I_{\rho+}(-m,\Phi) + \frac{\gamma_o\,m}{\omega\,\varepsilon_o} I_{z+}(-m,\Phi) \\ \xi\ I_{z+}(\eta,0) + \frac{\tau_o^2}{\omega\,\mu_o} V_{\rho+}(\eta,0) + \frac{\gamma_o\,\eta}{\omega\,\mu_o} V_{z+}(\eta,0) = -n\, I_{z+}(-m,\Phi) + \frac{\tau_o^2}{\omega\,\mu_o} V_{\rho+}(-m,\Phi) - \frac{\gamma_o\,m}{\omega\,\mu_o} V_{z+}(-m,\Phi) \end{cases} \tag{4}$$

$$\begin{cases} \xi\, V_{z+}(\eta,0) + \frac{\tau_o^2}{\omega\,\varepsilon_o} I_{\rho+}(\eta,0) + \frac{\gamma_o\,\eta}{\omega\,\varepsilon_o} I_{z+}(\eta,0) = -n\, V_{z+}(-m,-\Phi) + \frac{\tau_o^2}{\omega\,\varepsilon_o} I_{\rho+}(-m,-\Phi) - \frac{\gamma_o\,m}{\omega\,\varepsilon_o} I_{z+}(-m,-\Phi) \\ \xi\ I_{z+}(\eta,0) - \frac{\tau_o^2}{\omega\,\mu_o} V_{\rho+}(\eta,0) - \frac{\gamma_o\,\eta}{\omega\,\mu_o} V_{z+}(\eta,0) = -n\ I_{z+}(-m,-\Phi) - \frac{\tau_o^2}{\omega\,\mu_o} V_{\rho+}(-m,-\Phi) + \frac{\gamma_o\,m}{\omega\,\mu_o} V_{z+}(-m,-\Phi) \end{cases} \tag{5}$$

$$\begin{cases} -\xi_1\, V_{z+}(\eta,-\pi) + \frac{\tau_1^2}{\omega\,\varepsilon_1} I_{\rho+}(\eta,-\pi) + \frac{\gamma_1\,\eta}{\omega\,\varepsilon_1} I_{z+}(\eta,-\pi) = n_1\, V_{z+}(-m_1,-\Phi) + \frac{\tau_1^2}{\omega\,\varepsilon_1} I_{\rho+}(-m_1,-\Phi) - \frac{\gamma_1 m_1}{\omega\,\varepsilon_1} I_{z+}(-m_1,-\Phi) \\ -\xi_1\ I_{z+}(\eta,-\pi) - \frac{\tau_1^2}{\omega\,\mu_1} V_{\rho+}(\eta,-\pi) - \frac{\gamma_1\,\eta}{\omega\,\mu_1} V_{z+}(\eta,-\pi) = n_1\ I_{z+}(-m_1,-\Phi) - \frac{\tau_1^2}{\omega\,\mu_1} V_{\rho+}(-m_1,-\Phi) + \frac{\gamma_1\,m_1}{\omega\,\mu_1} V_{z+}(-m_1,-\Phi) \end{cases} \tag{6}$$

$$\begin{cases} \xi_1\, V_{z+}(\eta,\pi) + \frac{\tau_1^2}{\omega\,\varepsilon_1} I_{\rho+}(\eta,\pi) + \frac{\gamma_1\,\eta}{\omega\,\varepsilon_1} I_{z+}(\eta,\pi) = -n_1\ V_{z+}(-m_1,\Phi) + \frac{\tau_1^2}{\omega\,\varepsilon_1} I_{\rho+}(-m_1,\Phi) - \frac{\gamma_1\,m_1}{\omega\,\varepsilon_1} I_{z+}(-m_1,\Phi) \\ -\xi_1\ I_{z+}(\eta,\pi) + \frac{\tau_1^2}{\omega\,\mu_1} V_{\rho+}(\eta,\pi) + \frac{\gamma_1\,\eta}{\omega\,\mu_1} V_{z+}(\eta,\pi) = n_1\, I_{z+}(-m_1,\Phi) + \frac{\tau_1^2}{\omega\,\mu_1} V_{\rho+}(-m_1,\Phi) - \frac{\gamma_1\,m_1}{\omega\,\mu_1} V_{z+}(-m_1,\Phi) \end{cases} \tag{7}$$

In order to obtain a compact formulation of the problem we introduce the generalized factorization of the functions ξ, ξ_1, n and n_1 reported in [33]: generalized factorization means that $f(\eta) = f_+(\eta) f_-(m)$ and $f_1(\eta) = f_{1+}(\eta) f_{1-}(m_1)$.

The use of these factorizations and mathematical manipulations (sum and subtraction) of (4)-(7) yield a new system of equations where the η-plus functions for $\varphi = 0, \pi$ (*i.e.* the axial spectra $V_{z+}(\eta,0)$, $V_{z+}(\eta,\pi)$, $I_{\rho+}(\eta,0)$ and $I_{\rho+}(\eta,\pi)$) are determined in terms of m- and m_1-spectral functions defined for $\varphi = \pm\Phi$ (facial spectra). It yields a system of eight functional equations reported in (9) for $i = 1,3,5,7$.

$$\begin{cases} Y_{(i)+}(\eta) = X_{(i)+}(-m)\ - \frac{\xi_-}{n_+} X_{(i+1)+}(-m) \\ Y_{(i+1)+}(\eta) = \dot{X}_{(i)+}(-m_1)\ + \frac{\xi_{1-}}{n_{1+}} \dot{X}_{(i+1)+}(-m_1) \end{cases} \tag{9}$$

For the sake of brevity Table I reports all the plus/minus unknowns of (9) defined in terms of:

$$s_{ab+}(-c) = a_{b+}(-c,\Phi) + a_{b+}(-c,-\Phi) \tag{10}$$

$$d_{ab+}(-c) = a_{b+}(-c,\Phi) - a_{b+}(-c,-\Phi) \tag{11}$$

where $a = \{V,\, I\}$, $b = \{z,\, \rho\}$ and $c = \{m,\, m_1\}$.

Equations (9) are GWHE since the unknown functions are defined in different complex planes, *i.e.* η and m or m_1.

This system of equations are the Wiener-Hopf formulation of the problem under investigation.

A. Reduction of GWHE to CWHE

In order to solve the system of GWHE (9) where multiple complex planes coexist, we introduce the special mapping (12) defined in [33] and used in [36] to solve the equations for impenetrable wedge. This mapping is used to obtain CWHE in angular regions with aperture angle Φ_x and transverse component of the wave vector τ_x. The mapping is used in each equation of (9) depending on the appropriate angular region.

$$\eta = \eta(\bar{\eta}) = -\tau_x \cos\left(\frac{\Phi_x}{\pi} \arccos\left(-\frac{\bar{\eta}}{\tau_x}\right)\right) \tag{12}$$

With reference to Fig. 1, in regions 1 and 2 the correct mapping is the first of (13) and is applied to the first equations of (9), on the contrary in regions 3 and 4 the mapping is the second one of (13) and is applied to the second equations of (9).

$$\begin{aligned} \eta &= \eta(\alpha) = -\tau_o \cos\left(\tfrac{\Phi}{\pi} \arccos\left(-\tfrac{\alpha}{\tau_o}\right)\right) \\ \eta &= \eta(\beta) = -\tau_1 \cos\left(\tfrac{\Phi_1}{\pi} \arccos\left(-\tfrac{\beta}{\tau_1}\right)\right) \end{aligned} \tag{13}$$

This procedure yields a new system of eight equations

$$\begin{cases} \bar{Y}_{(i)+}(\alpha) = \bar{X}_{(i)-}(\alpha)\ - \frac{\xi_-}{n_+} \bar{X}_{(i+1)-}(\alpha) \\ \ddot{Y}_{(i+1)+}(\beta) = \ddot{X}_{(i)-}(\beta)\ + \frac{\xi_{1-}}{n_{1+}} \ddot{X}_{(i+1)-}(\beta) \end{cases} \tag{14}$$

with $i = 1,3,5,7$ and where the following notations have been used: $\bar{Y}_{(i)+}(\alpha) = Y_{(i)+}(\eta)$, $\bar{X}_{(i)-}(\alpha) = X_{(i)+}(-m)$, $\bar{X}_{(i+1)-}(\alpha) = X_{(i+1)+}(-m)$, and $\ddot{Y}_{(i+1)+}(\beta) = Y_{(i+1)+}(\eta)$, $\ddot{X}_{(i)-}(\beta) = X_{(i)+}(-m_1)$, $\ddot{X}_{(i+1)-}(\beta) = X_{(i+1)+}(-m_1)$. In (14) the terms, that combine the $\bar{X}_i$ and $\ddot{X}_i$ functions, constitute the matrix WH kernel of the system of equations whose elements are defined in two complex planes (α and β).

TABLE I
DEFINITIONS.

$Y_{1+}(\eta)$	$2\frac{\xi_+}{n_+} V_{z+}(\eta,0)$
$Y_{2+}(\eta)$	$2\frac{\xi_{1+}}{n_{1+}} V_{z+}(\eta,\pi)$
$X_{1+}(-m)$	$-\frac{n_-}{\xi_-} s_{vz+}(-m)$
$X_{2+}(-m)$	$\frac{1}{\xi_-^2}\left[\frac{\tau_o^2}{\omega\varepsilon} d_{i\rho+}(-m) - \frac{\gamma_o m}{\omega\varepsilon} d_{iz+}(-m)\right]$
$\dot{X}_{1+}(-m_1)$	$-\frac{n_{1-}}{\xi_{1-}} s_{vz+}(-m_1)$
$\dot{X}_{2+}(-m_1)$	$\frac{1}{\xi_{1-}^2}\left[\frac{\tau_1^2}{\omega\varepsilon_1} d_{i\rho+}(-m_1) - \frac{\gamma_o m_1}{\omega\varepsilon_1} d_{iz+}(-m_1)\right]$
$Y_{3+}(\eta)$	$\frac{2}{n_+\sqrt{\tau_o}}\left[-\frac{\tau_o^2}{\omega\varepsilon} I_{\rho+}(\eta,0) - \frac{\gamma_o\eta}{\omega\varepsilon} I_{z+}(\eta,0)\right]$
$Y_{4+}(\eta)$	$\frac{2}{n_{1+}\sqrt{\tau_1}}\left[\frac{\tau_1^2}{\omega\varepsilon_1} I_{\rho+}(\eta,-\pi) + \frac{\gamma_o\eta}{\omega\varepsilon_1} I_{z+}(\eta,-\pi)\right]$
$X_{3+}(-m)$	$-\frac{n_-}{\sqrt{\tau_o}} d_{vz+}(-m)$
$X_{4+}(-m)$	$\frac{1}{\sqrt{\tau_o}\xi_-}\left[\frac{\tau_o^2}{\omega\varepsilon} s_{i\rho+}(-m) - \frac{\gamma_o m}{\omega\varepsilon} s_{iz+}(-m)\right]$
$\dot{X}_{3+}(-m_1)$	$-\frac{n_{1-}}{\sqrt{\tau_1}} d_{vz+}(-m_1)$
$\dot{X}_{4+}(-m_1)$	$\frac{1}{\sqrt{\tau_1}\xi_{1-}}\left[\frac{\tau_1^2}{\omega\varepsilon_1} s_{i\rho+}(-m_1) - \frac{\gamma_o m_1}{\omega\varepsilon_1} s_{iz+}(-m_1)\right]$
$Y_{5+}(\eta)$	$-2\frac{\xi_+}{n_+} I_{z+}(\eta,0)$
$Y_{6+}(\eta)$	$-2\frac{\xi_{1+}}{n_{1+}} I_{z+}(\eta,\pi)$
$X_{5+}(-m)$	$\frac{n_-}{\xi_-} s_{iz+}(-m)$
$X_{6+}(-m)$	$\frac{1}{\xi_-^2}\left[\frac{\tau_o^2}{\omega\mu} d_{v\rho+}(-m) - \frac{\gamma_o m}{\omega\mu} d_{vz+}(-m)\right]$
$\dot{X}_{5+}(-m_1)$	$\frac{n_{1-}}{\xi_{1-}} s_{iz+}(-m_1)$
$\dot{X}_{6+}(-m_1)$	$\frac{1}{\xi_{1-}^2}\left[\frac{\tau_1^2}{\omega\mu_1} d_{v\rho+}(-m_1) - \frac{\gamma_o m_1}{\omega\mu_1} d_{vz+}(-m_1)\right]$
$Y_{7+}(\eta)$	$-\frac{2}{n_+\sqrt{\tau_o}}\left[\frac{\tau_o^2}{\omega\mu} V_{\rho+}(\eta,0) + \frac{\gamma_o\eta}{\omega\mu} V_{z+}(\eta,0)\right]$
$Y_{8+}(\eta)$	$\frac{2}{n_{1+}\sqrt{\tau_1}}\left[\frac{\tau_1^2}{\omega\mu_1} V_{\rho+}(\eta,\pi) + \frac{\gamma_o\eta}{\omega\mu_1} V_{z+}(\eta,\pi)\right]$
$X_{7+}(-m)$	$\frac{n_-}{\sqrt{\tau_o}} d_{iz+}(-m)$
$X_{8+}(-m)$	$\frac{1}{\sqrt{\tau_o}\xi_-}\left[\frac{\tau_o^2}{\omega\mu} s_{v\rho+}(-m) - \frac{\gamma_o m}{\omega\mu} s_{vz+}(-m)\right]$
$\dot{X}_{7+}(-m_1)$	$\frac{n_{1-}}{\sqrt{\tau_1}} d_{iz+}(-m_1)$
$\dot{X}_{8+}(-m_1)$	$\frac{1}{\sqrt{\tau_1}\xi_{1-}}\left[\frac{\tau_1^2}{\omega\mu_1} s_{v\rho+}(-m_1) - \frac{\gamma_o m_1}{\omega\mu_1} s_{vz+}(-m_1)\right]$

Note that from (8) and (13)

$$m = \tau_o \cos\left(\frac{\Phi}{\pi}\arccos\left(\frac{-\alpha}{\tau_o}\right)+\Phi\right) \tag{15}$$

$$m_1 = \tau_1 \cos\left(\frac{\Phi_1}{\pi}\arccos\left(\frac{-\beta}{\tau_1}\right)+\Phi_1\right) \tag{16}$$

We recall that the factorizations of functions ξ, n are studied in [33] and for the sake of readability we report them below:

$$n_+ = \sqrt{\frac{\tau_o-\alpha}{2}},\ n_{1+} = \sqrt{\frac{\tau_1-\beta}{2}} \tag{17}$$

$$\xi_- = -\sqrt{\frac{\tau_o+\alpha}{2}},\ \xi_{1-} = -\sqrt{\frac{\tau_1+\beta}{2}} \tag{18}$$

In (14) some of the Wiener-Hopf unknowns are *non-conventional*. We define *non-conventional* or *non-standard* plus (minus) Laplace transform, the functions $F_+(\eta)$ ($F_-(\eta)$) that presents singularities in the standard regularity half plane $\mathrm{Im}[\eta] \geq 0$ ($\mathrm{Im}[\eta] \leq 0$). The non-conventional singularities are typically poles arising from geometrical optics contributions. Since we suppose that there are no sources in the interior of the penetrable wedge, the unconventional unknowns are only the one defined in the exterior region, *i.e.* the unknowns defined in the α complex plane. We can intuitively deduce if a plus/minus η Laplace transform (2) of a plane wave is standard or not, by examining the direction and the orientation of its flow. If the Laplace transform is performed along a certain direction (for instance $\varphi = 0$ *i.e.* positive x axis) and the plane wave is flowing along the same direction but opposite orientation ($-x$ direction) we obtain a spectrum with a pole in the upper half-plane when the medium is supposed with small losses $Im[k_o] \lesssim 0$. In this case we obtain standard minus functions and non-standard plus functions.

B. Fredholm factorization

To obtain approximate solutions of the system of equations (14) we apply the Fredholm factorization method described in [34], [37]. This method reduces the WH equations to Fredholm integral equations using the contour integration and the Cauchy formula. The integral equations of the Fredholm factorization are written only in terms of conventional plus (minus) unknowns [37].

We recall that only the unknowns defined in the α complex plane can be non-conventional, since there are no sources in the interior of the penetrable wedge. The geometrical optic pole is $\alpha_o = -\tau_o \cos\left(\frac{\pi}{\Phi}\varphi_o\right)$, see [36]. This pole is related to three waves: the incident wave, the face a reflected wave and the face b reflected wave. The location of α_o in the α complex plane depends on φ_o. If $\varphi_o < \frac{\Phi}{2}$ ($\varphi_o > \frac{\Phi}{2}$) the α_o is located in the upper (lower) half of the α complex plane yielding unconventional plus (minus) unknowns with $Im[k_o] \lesssim 0$.

The extraction of non-conventional parts on the non-conventional WH unknowns yields the source terms in the Fredholm equations, see [37]. The source terms in the Fredholm equations are related to incident field and/or reflected fields as the associated poles α_o are located in the proper or improper sheet of the α-plane (see Appendix I of [36]). The associated poles α_o can be captured by contour integration only if they are located in the proper sheet of α. A complete discussion on the source terms of Fredholm equations is reported in Appendix I.

Using the Fredholm factorization method we obtain the system of integral equations (19) with $i = 1, 3, 5, 7$ and where the source terms $\bar{n}_i(\alpha)$ are described in Appendix I.

The complete solution of Wiener-Hopf problem is obtained in terms of the spectral unknowns by numerically solving the minus unknowns in (19). We note that the plus unknowns can be obtained through (14) or by using the equivalent integral representation available from (19):

$$\begin{cases} \bar{Y}_{(i)+}(\alpha) = \frac{1}{2\pi j}\int\limits_{-\infty}^{\infty} \frac{\left(\frac{\tau_o+\alpha'}{\sqrt{\tau_o^2-\alpha'^2}} - \frac{\tau_o+\alpha}{\sqrt{\tau_o^2-\alpha^2}}\right)\bar{X}_{(i+1)-}(\alpha')}{\alpha'-\alpha} d\alpha' + \bar{n}_i(\alpha) \\ \ddot{Y}_{(i+1)+}(\beta) = -\frac{1}{2\pi j}\int\limits_{-\infty}^{\infty} \frac{\left(\frac{\tau_1+\beta'}{\sqrt{\tau_1^2-\beta'^2}} - \frac{\tau_1+\beta}{\sqrt{\tau_1^2-\beta^2}}\right)\ddot{X}_{(i+1)-}(\beta')}{\beta'-\beta} d\beta' \end{cases} \tag{20}$$

C. Approximate solutions of the Fredholm equations

The numerical solution of the Fredholm integral equations (19) is obtained in several steps. Taking inspiration from the scheme already used in other problems, see [36] and [37], the steps are:

- formulation of the Fredholm equations in the angular complex plane w,
- introduction of contour deformation to enhance the convergence of the Fredholm equations,
- introduction of mapping to relate the unknowns defined the inner and the outer of the wedge [41],
- numerical discretization of the equation and numerical representation of the solution in the angular plane w,
- analytic continuation of the approximate solutions through recursive equations in the angular complex plane.

The angular complex plane w is particulary useful to estimate the far field components (Section IV) as already shown in [36] for the impenetrable wedge case. Since the Fredholm integral equations (19) are written into two complex planes (α and β), we need to define two angular complex planes and two modified angular complex planes (the overlined ones) respectively related to quantities defined in the free space region and in the isotropic penetrable region:

$$\begin{aligned} \alpha &= -\tau_o \cos\tfrac{\pi}{\Phi} w = -\tau_o \cos\bar{w} \\ \beta &= -\tau_1 \cos\tfrac{\pi}{\Phi_1} w_1 = -\tau_1 \cos\bar{w}_1 \end{aligned} \tag{21}$$

with $\bar{w} = \frac{\pi}{\Phi} w$ and $\bar{w}_1 = \frac{\pi}{\Phi} w_1$.

The properties and the inverse transformations of the mappings are reported in Appendix I of [36]. We recall that in the angular complex planes (w or w_1), all the plus functions are even functions [33], [42]. From (13) and (21) we obtain the Snell law in the spectral domain

$$\eta = -\tau_o \cos w = -\tau_1 \cos w_1 \tag{22}$$

We assert that α_o may represent three different waves (the incident wave, the face a reflected wave and the face b reflected wave) that have three different representation in w-plane: see Appendix I.

$$\begin{cases} \bar{X}_{(i)-}(\alpha) + \frac{\tau_o+\alpha}{\sqrt{\tau_o^2-\alpha^2}}\bar{X}_{(i+1)-}(\alpha) - \frac{1}{2\pi j}\int\limits_{-\infty}^{\infty} \frac{\left(\frac{\tau_o+\alpha'}{\sqrt{\tau_o^2-\alpha'^2}} - \frac{\tau_o+\alpha}{\sqrt{\tau_o^2-\alpha^2}}\right)\bar{X}_{(i+1)-}(\alpha')}{\alpha'-\alpha} d\alpha' = \bar{n}_i(\alpha) \\ \ddot{X}_{(i)-}(\beta) - \frac{\tau_1+\beta}{\sqrt{\tau_1^2-\beta^2}}\ddot{X}_{(i+1)-}(\beta) + \frac{1}{2\pi j}\int\limits_{-\infty}^{\infty} \frac{\left(\frac{\tau_1+\beta'}{\sqrt{\tau_1^2-\beta'^2}} - \frac{\tau_1+\beta}{\sqrt{\tau_1^2-\beta^2}}\right)\ddot{X}_{(i+1)-}(\beta')}{\beta'-\beta} d\beta' = 0 \end{cases} \tag{19}$$

Given (8), (17), (18) the following representations hold in the w and w_1 ($\bar{w}$ and $\bar{w}_1$) planes:

$$\begin{array}{cc} \xi = -\tau_o \sin w & \xi_1 = -\tau_1 \sin w_1 \\ m = \tau_o \cos(w+\Phi) & m_1 = \tau_1 \cos(w_1+\Phi_1) \\ n = \tau_o \sin(w+\Phi) & n_1 = \tau_1 \sin(w_1+\Phi_1) \\ n_+ = \sqrt{\tau_o}\cos\frac{\bar{w}}{2} & n_{1+} = \sqrt{\tau_1}\cos\frac{\bar{w}_1}{2} \\ \xi_- = \sqrt{\tau_o}\sin\frac{\bar{w}}{2} & \xi_{1-} = \sqrt{\tau_1}\sin\frac{\bar{w}_1}{2} \end{array} \tag{23}$$

In the following we will use the notations (24) for the axial spectral unknowns $F(\eta)$ defined in different spectral domains: outer (inner) axial refers to direction $\varphi = 0$ ($\varphi = \pi$).

$$\begin{array}{l} F(\eta) = F(-\tau_o\cos w) = \hat{F}(w) = \bar{F}(\alpha) = \bar{F}(-\tau_o\cos\bar{w}) \\ F_\pi(\eta) = F_\pi(-\tau_1\cos w_1) = \hat{F}_\pi(w_1) = \ddot{F}_\pi(\beta) = \ddot{F}_\pi(-\tau_1\cos\bar{w}_1) \end{array} \tag{24}$$

A similar notation is applied to quantities with second argument φ (spectral unknowns for arbitrary direction φ), for example $F(\eta,\varphi) = \hat{F}(w,\varphi)$.

The second step of the procedure allows a fast convergence of the Fredholm equations by contour deformation. The real axis contours in the first and second equations of (19) are warped into straight lines that join the $\pm j\tau_o$ and $\pm j\tau_1$ respectively in the α and β planes. These straight lines λ_α and λ_β correspond to the two lines respectively in the $\bar{w}$ and $\bar{w}_1$ planes parameterized by

$$\lambda_\alpha:\ \bar{w} = -\frac{\pi}{2} + j\,u,\ \ \lambda_\beta:\ \bar{w}_1 = -\frac{\pi}{2} + j\,v \tag{25}$$

with real u, v. Therefore we have:

$$\alpha(u) = -\tau_o\cos\left(-\frac{\pi}{2} + ju\right),\ \beta(v) = -\tau_1\cos\left(-\frac{\pi}{2} + jv\right) \tag{26}$$

The system of equations (19) become (27) with $i = 1,3,5,7$ and where $P_i(u)$, $Q_i(v)$, $M(u,u')$, $n_i(u)$ are defined in (28).

$$\begin{cases} P_i(u) = \tau_o X_{i+}(\tau_o\cos\left[\frac{\Phi}{\pi}\left(-\frac{\pi}{2}+ju\right)+\Phi\right]) \\ Q_i(v) = \tau_o \dot{X}_{i+}(\tau_1\cos\left[\frac{\Phi_1}{\pi}\left(-\frac{\pi}{2}+jv\right)+\Phi_1\right]) \\ M(u,u') = \frac{e^u}{(e^u-j)}\frac{e^{u'}+j}{e^{u+u'}+1} \\ n_i(u) = \bar{n}_i(\alpha(u)) \end{cases} \tag{28}$$

We observe that the second equations in (27) are valid in the whole complex v-plane through analytical continuation. By enforcing the constraint $m = m_1$ (third step) we obtain the following complex mapping between u-plane and v-plane:

$$v = v(u) = \frac{j\pi}{2\Phi_1}\left(\Phi_1 - 2\arccos\frac{\cos\frac{(\pi+2j\,u)\Phi}{2\pi}}{\sqrt{\varepsilon_{tr}}}\right) \tag{29}$$

where $\varepsilon_{tr} = (\tau_1/\tau_o)^2$. The mapping (29) enforces in (27) the same parameterization of the spectral quantities (10)-(11) defined on the faces and in particular the parameterization of the spectral voltages and currents for $\varphi = \pm\Phi$: $V_{z+}(-m,\pm\Phi) = V_{z+}(-m_1,\pm\Phi)$ and $I_{\rho+}(-m,\pm\Phi) = I_{\rho+}(-m_1,\pm\Phi)$. The purpose of this procedure is to obtain a solvable system of equations whose unknowns are consistent: for example in terms of the $P_i(u)$ avoiding $Q_i(v)$.

Since the integral term in the second equations of (27) is performed along the real axis of the v-plane (that corresponds to a curve in the complex u-plane), we need to estimate the quantities $Q_{i+1}(v)$ in terms of the functions $P_{i+1}(u)$. This requirement is achieved through the application of the Cauchy formula:

$$f(m_1(v)) = \frac{1}{2\pi j}\oint\limits_\gamma \frac{f(m)}{m-m_1(v)}dm = \frac{1}{2\pi j}\int\limits_{-\infty}^{\infty}\frac{f(m(u'))}{m(u')-m_1(v)}\frac{dm(u')}{du'}du' \tag{30}$$

where

$$\begin{cases} m(u) = k\cos\left[\frac{\Phi}{\pi}\left(-\frac{\pi}{2}+ju\right)+\Phi\right] \\ m_1(v) = k_1\cos\left[\frac{\Phi_1}{\pi}\left(-\frac{\pi}{2}+jv\right)+\Phi_1\right] \end{cases} \tag{31}$$

The fourth step is efficiently implemented using simple quadrature rules as demonstrated in [36] for impenetrable wedges. Finally the analytic continuation of the solution is achieved using recursive equations obtained from the WH formulation (4)-(7) written in the angular domains w and w_1.

For the sake of simplicity, in the following, we develop the procedure to obtain the numerical solution for the particular case of diffraction of an E-polarized plane wave by a dielectric wedge at normal incidence.

III. Numerical implementation: E-polarized plane wave at normal incidence

Since we are dealing with an E-polarized plane wave at normal incidence on a dielectric wedge ($H_o = 0$, $\delta = \frac{\pi}{2}$, $\mu_r = 1$, $\Phi < \pi/2$ *i.e.* acute wedge), all the equations reported above are simplified, although the procedure to derive the solution remains similar. In particular the equations reported in the previous sections are valid with the simplified explicit definitions reported in Table II. Note that $\tau_o = k_o$, $\tau_1 = k_1$, $\gamma_o = \gamma_1 = 0$, $Z_o = \sqrt{\frac{\mu_o}{\varepsilon_o}}$, $Z_1 = \sqrt{\frac{\mu_o}{\varepsilon_o\varepsilon_r}}$, $\varepsilon_{tr} = \varepsilon_r$, while $Y_{i+}(\eta)$, $X_{i+}(-m)$, $\dot{X}_{i+}(-m_1)$ are null for $i = 5,6,7,8$ and therefore (27) are not trivial only for $i = 1,3$.

Let us consider (27) for $i = 1,3$. Using (28), the definitions of Table II, (23) and (25) we obtain that:

$$Q_1(v(u)) = \frac{n_{1-}}{\xi_{1-}}\frac{\xi_-}{n_-}P_1(u) \tag{32}$$

i.e. explicitly

$$Q_1(v(u)) = \frac{\cosh(u)\sin[-\frac{(-jv(u)+\frac{\pi}{2})\Phi_1}{\pi}+\Phi_1]}{\cosh(v(u))\,\sin[-\frac{(-ju+\frac{\pi}{2})\Phi}{\pi}+\Phi]}P_1(u) \tag{33}$$

Similarly we obtain:

$$Q_2(v(u)) = \frac{Z_1\sin^2[\frac{1}{2}(-\frac{\pi}{2}+ju)]}{Z_o\sin^2[\frac{1}{2}(-\frac{\pi}{2}+jv(u))]}P_2(u) \tag{34}$$

$$Q_3(v(u)) = \frac{\cos[\frac{1}{2}(-\frac{\pi}{2}+ju)]\sin[-\frac{jv(u)\Phi_1}{\pi}+\frac{\Phi_1}{2}]}{\cos[\frac{1}{2}(-\frac{\pi}{2}+jv(u))]\sin[\frac{ju\Phi}{2}+\frac{\Phi}{2}]}P_3(u) \tag{35}$$

$$Q_4(v(u)) = \frac{Z_1\sin[\frac{1}{2}(-\frac{\pi}{2}+ju)]}{Z_o\sin[\frac{1}{2}(-\frac{\pi}{2}+jv(u))]}P_4(u) \tag{36}$$

$$\begin{cases} P_i(u) - \tan\frac{-\pi/2+ju}{2} P_{i+1}(u) - \frac{1}{\pi j}\int_{-\infty}^{\infty} M(u,u')P_{i+1}(u')du' = n_i(u) \\ Q_i(v) + \tan\frac{-\pi/2+jv}{2} Q_{i+1}(v) + \frac{1}{\pi j}\int_{-\infty}^{\infty} M(v,v')Q_{i+1}(v')dv' = 0 \end{cases} \tag{27}$$

TABLE II
DEFINITIONS FOR E-POLARIZED PLANE WAVE AT NORMAL INCIDENCE.

$Y_{1+}(\eta)$	$2\frac{\xi_+}{n_+} V_{z+}(\eta,0)$
$Y_{2+}(\eta)$	$2\frac{\xi_{1+}}{n_{1+}} V_{z+}(\eta,\pi)$
$X_{1+}(-m)$	$-\frac{n_-}{\xi_-}\left[V_{z+}(-m,\Phi) + V_{z+}(-m,-\Phi)\right]$
$X_{2+}(-m)$	$\frac{1}{\xi_-^2} k_o Z_o \left[I_{\rho+}(-m,\Phi) - I_{\rho+}(-m,-\Phi)\right]$
$\dot{X}_{1+}(-m_1)$	$-\frac{n_{1-}}{\xi_{1-}}\left[V_{z+}(-m_1,\Phi) + V_{z+}(-m_1,-\Phi)\right]$
$\dot{X}_{2+}(-m_1)$	$\frac{1}{\xi_{1-}^2} k_1 Z_1 \left[I_{\rho+}(-m_1,\Phi) - I_{\rho+}(-m_1,-\Phi)\right]$
$Y_{3+}(\eta)$	$\frac{-2\sqrt{k_o}}{n_+} Z_o I_{\rho+}(\eta,0)$
$Y_{4+}(\eta)$	$\frac{2\sqrt{k_1}}{n_{1+}} Z_1 I_{\rho+}(\eta,-\pi)$
$X_{3+}(-m)$	$-\frac{n_-}{\sqrt{k_o}}\left[V_{z+}(-m,\Phi) - V_{z+}(-m,-\Phi)\right]$
$X_{4+}(-m)$	$\frac{\sqrt{k_o}}{\xi_-} Z_o \left[I_{\rho+}(-m,\Phi) + I_{\rho+}(-m,-\Phi)\right]$
$\dot{X}_{3+}(-m_1)$	$-\frac{n_{1-}}{\sqrt{k_1}}\left[V_{z+}(-m_1,\Phi) - V_{z+}(-m_1,-\Phi)\right]$
$\dot{X}_{4+}(-m_1)$	$\frac{\sqrt{k_1}}{\xi_{1-}} Z_1 \left[I_{\rho+}(-m_1,\Phi) + I_{\rho+}(-m_1,-\Phi)\right]$

As reported in step 4 of the previous section, in order to obtain a solvable system of equations from (27), we need to estimate the quantities $Q_{i+1}(v)$ in terms of the functions $P_{i+1}(u)$. We recall that this procedure is required for the evaluation of the integral term in the second equations of (27).

This requirement is achieved through the application of the Cauchy formula (30), explicitly reported below:

$$Q_{2,4}(v') = \int_{-\infty}^{\infty} \Psi_{2,4}(v',u') P_{2,4}(u') du' \tag{37}$$

where

$$\begin{cases} \Psi_2(v,u) = -\frac{\Phi Z_1 \sin^2[-\frac{\pi}{4}+\frac{ju}{4}]}{2\pi^2 Z_o \sin^2[-\frac{\pi}{4}+\frac{jv}{4}]} \frac{\sin[\frac{\Phi}{\pi}(ju+\frac{3\pi}{2})]}{\cos[\frac{\Phi}{\pi}(ju+\frac{3\pi}{2})] - \sqrt{\varepsilon_r}\cos[\frac{\Phi_1}{\pi}(jv+\frac{3\pi}{2})]} \\ \Psi_4(v,u) = \Psi_2(v,u)\frac{\sin[\frac{1}{2}(-\frac{\pi}{2}+jv)]}{\sin[\frac{1}{2}(-\frac{\pi}{2}+ju)]} \end{cases} \tag{38}$$

By substituting (33)-(36) in (27) we obtain, with the use of (37), two decoupled explicit systems of equations (39) amenable to be solved numerically in terms of $P(u)$ functions.

Note that the quantities $n_1(u)$ and $n_3(u)$ are related to the E-polarized incident wave (see Appendix I for details), and when the plus unknowns are non-standard ($0 < \varphi_o < \frac{\Phi}{2}$)

$$n_i(u) = -\frac{\bar{T}_{oi}}{(j\sinh u - \cos\frac{\pi}{\Phi}\varphi_o)}, \quad i = 1,3 \tag{40}$$

with $\bar{T}_{o1}$ and $\bar{T}_{o3}$ defined in Appendix I.

Efficient approximate methods for the solution of Fredholm equations of second kind are widely available in the literature, see for example [43].

Since the kernel of (39) presents a well suited behavior, we use a simple sample and quadrature scheme to obtain accurate and stable numerical solutions. We apply uniform sampling $f(h\,i)$ with $i = -\frac{A}{h}..\frac{A}{h}$ and modified left-rectangle numerical integration formula $\int_{-\infty}^{\infty} f(u)du \approx h \sum_{i=-A/h}^{A/h} f(h\,i)$ where A and h are respectively the truncation parameter and the step parameter for the integrals in u. This rule has been successfully applied for the impenetrable wedge case [36]. The total number of samples is $N = 2A/h + 1$. We observe that as $A \to +\infty$ and $h \to 0$, the numerical solution of the Fredholm integral equation converges to the exact solution [43]; consequently h has to be chosen as small as possible and A has to be chosen as large as possible.

For instance, according to our experience, we assume $A = A_1 = 10$ and $h = h_1 = 0.05$ (A_1 and h_1 are related to the second and fourth equations in (39)) to get stable solutions which provide very accurate values in terms of $P_i(u)$ and $Q_i(v)$ samples, voltages' and currents' spectra and field components, see Section V.

The discretized form of equations (39) is reported below:

$$\begin{cases} \begin{cases} \mathbf{I}\underline{P_1} + \mathbf{D_{12}}\underline{P_2} + \mathbf{K_{12}}\underline{P_2} = \underline{n_1} \\ \mathbf{D_{21}}\underline{P_1} + \mathbf{D_{22}}\underline{P_2} + \mathbf{K_{22}}\underline{Q_2} = \underline{0} \end{cases} \\ \begin{cases} \mathbf{I}\underline{P_3} + \mathbf{D_{34}}\underline{P_4} + \mathbf{K_{34}}\underline{P_4} = \underline{n_3} \\ \mathbf{D_{43}}\underline{P_3} + \mathbf{D_{44}}\underline{P_4} + \mathbf{K_{44}}\underline{Q_4} = \underline{0} \end{cases} \end{cases} \tag{41}$$

where we need to use the discretized form of (37):

$$\underline{Q_{2,4}} = \mathbf{\Psi_{2,4}}\underline{P_{2,4}} \tag{42}$$

With reference to the system of equations (39), in (41):

- $\underline{P_i}$ is the column vector containing the samples of $P_i(u)$ function,
- $\mathbf{I}$ is the identity matrix,
- $\mathbf{D_{ij}}$ is the diagonal matrix that represents the function multiplying $P_j(u)$ in equation number i,
- $\mathbf{K_{ij}}$ is a full matrix that represents the kernel in equation number i that multiplies $P_j(u')$ or $Q_j(v')$,
- $\mathbf{\Psi_{2,4}}$ is a full matrix that represents the operators (38),
- $\underline{n_i}$ is the column vector containing the samples of the source in equation number i.

All the matrices and vector quantities are of dimension N. Simple algebraic manipulations allow to obtain two linear systems of dimension N where the unknowns are only $\underline{P_2}$ and $\underline{P_4}$.

The physical plus WH spectral unknowns $V_{z+}(\eta,0)$, $V_{z+}(\eta,\pi)$, $I_{\rho+}(\eta,0)$ and $I_{\rho+}(\eta,\pi)$ are reconstructed in the w and w_1 planes (respectively $\hat{V}_+(w)$, $\hat{V}_{\pi+}(w_1)$, $\hat{I}_+(w)$ and $\hat{I}_{\pi+}(w_1)$) via the sampling of (20) and using the definitions of Table II and (23): see (43)-(46) for the explicit formula where $Q_{2,4}(h_1 i)$ are obtained through (42) and non-standard plus unknown are considered, *i.e.* $0 < \varphi_o < \frac{\Phi}{2}$. Note that the discretization of kernel $M(u,u')$ in (39) yields artificial poles in (43)-(46) due to the zeros of $(e^{u+u'}+1)$ when $u' = hi$. These poles correspond to spurious singularities on the axial spectra for $w = -\frac{3}{2}\Phi - j\frac{\Phi}{\pi}hi$ and $w_1 = -\frac{3}{2}\Phi_1 - j\frac{\Phi_1}{\pi}h_1 i$.

Since the solution is obtained via numerical procedure along the lines λ_α and λ_β (25), *i.e.* the vertical lines $\mathrm{Re}[\bar{w}] = -\frac{\pi}{2}$ ($\mathrm{Re}[w] = -\frac{\Phi}{2}$) and $\mathrm{Re}[\bar{w}_1] = -\frac{\pi}{2}$ ($\mathrm{Re}[w_1] = -\frac{\Phi_1}{2}$), the two pairs of equations (43), (45) and (44), (46) provide only analytical elements of the axial spectra. We define the *starting spectra* as the axial spectra respectively in the regularity strips

$$\begin{cases} P_1(u) - \tan\frac{-\frac{\pi}{2}+ju}{2} P_2(u) - \frac{1}{\pi j}\int\limits_{-\infty}^{\infty} M(u,u')P_2(u')du' = n_1(u) \\ \frac{\cosh(u)\sin[\frac{jv(u)\Phi_1}{\pi}+\frac{\Phi_1}{2}]P_1(u)}{\cosh(v(u))\,\sin[\frac{ju\,\Phi}{\pi}+\frac{\Phi}{2}]} + \tan\frac{-\frac{\pi}{2}+jv(u)}{2}\frac{Z_1\sin^2[\frac{1}{2}(-\frac{\pi}{2}+ju)]P_2(u)}{Z_o\sin^2[\frac{1}{2}(-\frac{\pi}{2}+jv(u))]} + \frac{1}{\pi j}\int\limits_{-\infty}^{\infty} M(v(u),v')Q_2(v')dv' = 0 \\ P_3(u) - \tan\frac{-\frac{\pi}{2}+ju}{2} P_4(u) - \frac{1}{\pi j}\int\limits_{-\infty}^{\infty} M(u,u')P_4(u')du' = n_3(u) \\ \frac{\cos[\frac{1}{2}(-\frac{\pi}{2}+ju)]\sin[\frac{jv(u)\Phi_1}{\pi}+\frac{\Phi_1}{2}]P_3(u)}{\cos[\frac{1}{2}(-\frac{\pi}{2}+jv(u))]\sin[\frac{ju\,\Phi}{\pi}+\frac{\Phi}{2}]} + \tan\frac{-\frac{\pi}{2}+jv(u)}{2}\frac{Z_1\sin[\frac{1}{2}(-\frac{\pi}{2}+ju)]P_4(u)}{Z_o\sin[\frac{1}{2}(-\frac{\pi}{2}+jv(u))]} + \frac{1}{\pi j}\int\limits_{-\infty}^{\infty} M(v(u),v')Q_4(v')dv' = 0 \end{cases} \tag{39}$$

$$\hat{V}_+(w) = V_{z+}(-k_o\cos w, 0) = -\frac{\sin(\frac{\pi w}{\Phi})}{4k_o\sin w}\left\{\frac{h}{\pi j}\sum_{i=-\frac{A}{h}}^{\frac{A}{h}} M\left[-j(\frac{\pi w}{\Phi}+\frac{\pi}{2}), hi\right]P_2(hi) - \frac{\bar{T}_{o1}}{\cos\frac{\pi w}{\Phi}-\cos\frac{\pi\varphi_o}{\Phi}}\right\} \tag{43}$$

$$\hat{V}_{\pi+}(w_1) \quad = V_{z+}(-k_1\cos w_1, \pi) = \frac{\sin(\frac{\pi}{\Phi_1}w_1)}{4k_o\sin w_1}\left\{\frac{h_1}{\pi j}\sum_{i=-\frac{A_1}{h_1}}^{\frac{A_1}{h_1}} M\left[-j(\frac{\pi w_1}{\Phi_1}+\frac{\pi}{2}), h_1 i\right]Q_2(h_1 i)\right\} \tag{44}$$

$$\hat{I}_+(w) = I_{\rho+}(-k_o\cos w, 0) = -\frac{\cos(\frac{\pi w}{2\Phi})}{2k_o Z_o}\left\{\frac{h}{\pi j}\sum_{i=-\frac{A}{h}}^{\frac{A}{h}} M\left[-j(\frac{\pi w}{\Phi}+\frac{\pi}{2}), hi\right]P_4(hi) - \frac{\bar{T}_{o3}}{\cos\frac{\pi w}{\Phi}-\cos\frac{\pi\varphi_o}{\Phi}}\right\} \tag{45}$$

$$\hat{I}_{\pi+}(w_1) = I_{\rho+}(-k_1\cos w_1, \pi) = -\frac{\cos(\frac{\pi w_1}{2\Phi_1})}{2k_o Z_1}\left\{\frac{h_1}{\pi j}\sum_{i=-\frac{A_1}{h_1}}^{\frac{A_1}{h_1}} M\left[-j(\frac{\pi w_1}{\Phi_1}+\frac{\pi}{2}), h_1 i\right]Q_4(h_1 i)\right\} \tag{46}$$

$-\Phi \le \mathrm{Re}[w] \le 0$ ($-\pi \le \mathrm{Re}[\bar{w}] \le 0$) and $-\Phi_1 \le \mathrm{Re}[w_1] \le 0$ ($-\pi \le \mathrm{Re}[\bar{w}_1] \le 0$). Note that the starting spectra show only the pole singularity of the incident field. Another important property is that the regularity segment $-\Phi \le w \le 0$ ($-\Phi_1 \le w_1 \le 0$) belongs to the proper sheet P_w (P_{w_1}) as defined in Appendix I of [36].

To apply the above procedure it is important to study the behavior at infinity of the spectra. This was accomplished in [41] and for the sake of brevity it is not reported here.

In order to obtain the global spectra in w and w_1 planes we need analytical continuations of the numerically approximated analytical elements. We note that if the problem were solved analytically, the closed form solution would be valid in the entire w and w_1 complex planes. However this is not possible in the general case of an isotropic penetrable wedge with arbitrary aperture angle.

The analytical continuation of the numerical results is an old and cumbersome problem of applied mathematics that can be approached in various ways. In this work we resort to recursive equations obtained representing the GWHE (9) of the problem in the w and w_1 planes using Table II and (22)-(23). By using the continuity relation (100) and eliminating the spectral unknowns defined at the interface $\varphi = \pm\Phi$, we obtain (53) where we have defined the functions

$$\hat{V}_d(w) = \sin(w)\hat{V}_+(w) \tag{47}$$

$$\hat{V}_{\pi d}(w_1) = \sin(w_1)\hat{V}_{\pi+}(w_1) \tag{48}$$

and where we have introduced the $g(w)$ and $g_1(w_1)$ functions derived from (22) and described in Appendix II:

$$w_1 = g(w) = -\arccos\left(\frac{\cos w}{\sqrt{\varepsilon_r}}\right) \tag{49}$$

$$w = g_1(w_1) = -\arccos\left(\sqrt{\varepsilon_r}\cos w_1\right) \tag{50}$$

Since plus functions are even functions in the angular planes w or w_1 [42], we assert that $\hat{V}_d(w)$ and $\hat{V}_{\pi d}(w_1)$ are odd. The symmetry properties of plus/minus functions together with (53) ensure the analytical continuation of $\hat{V}_+(w)$, $\hat{V}_{\pi+}(w_1)$, $\hat{I}_+(w)$ and $\hat{I}_{\pi+}(w_1)$. For instance, let us consider $\hat{V}_{\pi d}(w_1)$ ($\hat{V}_d(w)$). Its correct evaluation for each w_1 (w) is obtained through the approximate analytical element $\hat{V}_{\pi d}^{(num)}(w_1)$ ($\hat{V}_d^{(num)}(w)$) valid in $-\Phi_1 \le \mathrm{Re}[w_1] \le 0$ ($-\Phi \le \mathrm{Re}[w] \le 0$):

$$V_{\pi d}(w_1) = \begin{cases} V_{\pi d}^{(num)}(w_1) & -\Phi_1 \le \mathrm{Re}[w_1] \le 0 \\ -V_{\pi d}(-w_1) & \mathrm{Re}[w_1] > 0 \\ 2^{nd}eq.in(53) & \mathrm{Re}[w_1] < -\Phi_1 \end{cases} \tag{51}$$

$$V_d(w) = \begin{cases} V_d^{(num)}(w) & -\Phi \le \mathrm{Re}[w] \le 0 \\ -V_d(-w) & \mathrm{Re}[w] > 0 \\ 1^{st}eq.in(53) & \mathrm{Re}[w] < -\Phi \end{cases} \tag{52}$$

Note that the recursive formula (53) of the π axial unknowns ($\varphi = \pi$) with real argument w_1 requires the evaluation of the axial unknowns $\varphi = 0$ with complex arguments w, see Appendix II and test case 1 in Section V.

The use of rotating waves [44] enables us to represent in the angular complex planes (w and w_1) the Laplace transforms of the spectral unknowns for a direction φ in terms of the axial spectra

$$\begin{aligned} \hat{V}_d(w,\varphi) &= \frac{Z_o\left[\hat{I}_+(w-\varphi)-\hat{I}_+(w+\varphi)\right]+\hat{V}_d(w-\varphi)+\hat{V}_d(w+\varphi)}{2} \\ \hat{I}_+(w,\varphi) &= \frac{Z_o\left[\hat{I}_+(w-\varphi)+\hat{I}_+(w+\varphi)\right]+\hat{V}_d(w-\varphi)-\hat{V}_d(w+\varphi)}{2Z_o} \\ \hat{V}_{\pi d}(w_1,\varphi_1) &= \frac{Z_1\left[\hat{I}_{\pi+}(w_1+\varphi_1)-\hat{I}_{\pi+}(w_1-\varphi_1)\right]+\hat{V}_{\pi d}(w_1+\varphi_1)+\hat{V}_{\pi d}(w_1-\varphi_1)}{2} \\ \hat{I}_+(w_1,\varphi_1) &= \frac{Z_1\left[\hat{I}_{\pi+}(w_1+\varphi_1)+\hat{I}_{\pi+}(w_1-\varphi_1)\right]+\hat{V}_{\pi d}(w_1+\varphi_1)-\hat{V}_{\pi d}(w_1-\varphi_1)}{2Z_1} \end{aligned} \tag{54}$$

where we have defined the auxiliary quantities:

$$\begin{aligned} \hat{V}_d(w,\varphi) &= \sin(w)\hat{V}_+(w,\varphi) \\ \hat{V}_{\pi d}(w_1,\varphi_1) &= \sin(w_1)\hat{V}_+(w_1,\varphi_1) \end{aligned} \tag{55}$$

We observe that the quantities defined inside the dielectric wedge ($0 < |\varphi_1| < \Phi_1$) can be derived using symmetry from the quantities defined outside the wedge ($0 < |\varphi| < \Phi$) using the following substitutions:

$$\begin{gathered} \varphi \to -\varphi_1,\ w \to w_1,\ \Phi \to \Phi_1,\ k_o \to k_1,\ Z_o \to Z_1 \\ \{\hat{V}_+(w), \hat{I}_+(w)\} \to \{\hat{V}_{\pi+}(w_1), \hat{I}_{\pi+}(w_1)\} \end{gathered} \tag{56}$$

$$\begin{cases} \hat{V}_d(w) = \frac{Z_1\sin(w+\Phi)-Z_o\sin(g(w+\Phi))}{Z_1\sin(w+\Phi)+Z_o\sin(g(w+\Phi))}\hat{V}_d(w+2\Phi) + \frac{2Z_o\sin(w+\Phi)}{[Z_1\sin(w+\Phi)+Z_o\sin(g(w+\Phi))]}\hat{V}_{\pi d}(g(w+\Phi)+\Phi_1) \\ \hat{V}_{\pi d}(w_1) = \frac{2Z_1\sin(w_1+\Phi_1)}{[Z_1\sin(g_1(w_1+\Phi_1)+Z_o\sin(w_1+\Phi_1)]}\hat{V}_d(g_1(w_1+\Phi_1)+\Phi) - \frac{Z_1\sin(g_1(w_1+\Phi_1))-Z_o\sin(w_1+\Phi_1)}{Z_1\sin(g_1(w_1+\Phi_1))+Z_o\sin(w_1+\Phi_1)}\hat{V}_{\pi d}(w_1+2\Phi_1) \\ \hat{I}_+(w) = -\frac{Z_1\sin(w+\Phi)-Z_o\sin(g(w+\Phi))}{Z_1\sin(w+\Phi)+Z_o\sin(g(w+\Phi))}\hat{I}_+(w+2\Phi) + \frac{2Z_1\sin(w+\Phi)}{Z_1\sin(w+\Phi)+Z_o\sin(g(w+\Phi))}\hat{I}_{\pi+}(g(w+\Phi)+\Phi_1) \\ \hat{I}_{\pi+}(w_1) = \frac{2Z_o\sin(w_1+\Phi_1)}{Z_1\sin(g_1(w_1+\Phi_1))+Z_o\sin(w_1+\Phi_1)}\hat{I}_+(g_1(w_1+\Phi_1)+\Phi) + \frac{Z_1\sin(g_1(w_1+\Phi_1))-Z_o\sin(w_1+\Phi_1)}{Z_1\sin(g_1(w_1+\Phi_1))+Z_o\sin(w_1+\Phi_1)}\hat{I}_{\pi+}(w_1+2\Phi_1) \end{cases} \quad (53)$$

IV. Far-Field Evaluation

This section is devoted to the evaluation of the far-field pattern inside and outside the wedge. For the sake of simplicity we refer to a dielectric wedge structure illuminated by an E-polarized plane wave at normal incidence, generalization to skew incidence can be extrapolated from [36] where the impenetrable wedge is discussed. In this section we make reference to the evaluation of the exact field components in the exterior region $|\varphi| < \Phi$. Note that the procedure can be extended to the evaluation of the field in the interior region $|\varphi_1| < \Phi_1$ through the symmetry relations (56).

The exact total field is given by the following inverse Laplace transforms:

$$\begin{array}{l} E_z(\rho,\varphi) = \frac{1}{2\pi}\int_{B_r} V_{z+}(\eta,\varphi)e^{-j\eta\rho}d\eta \\ H_\rho(\rho,\varphi) = \frac{1}{2\pi}\int_{B_r} I_{\rho+}(\eta,\varphi)e^{-j\eta\rho}d\eta \end{array} \quad (57)$$

where B_r is the Bromwich contour for $V_{z+}(\eta,\varphi)$, $I_{\rho+}(\eta,\varphi)$. We recall that the singularities of standard plus functions are located in the lower η half-plane. In this case B_r is any arbitrary horizontal line located in the upper η half plane.

By introducing the w-plane ($\eta = -k_o\cos w$) we obtain:

$$\begin{array}{l} E_z(\rho,\varphi) = \frac{k_o}{2\pi}\int_{\lambda(B_r)} \hat{V}_+(w,\varphi)e^{jk_o\rho\cos w}\sin w dw \\ H_\rho(\rho,\varphi) = \frac{k_o}{2\pi}\int_{\lambda(B_r)} \hat{I}_+(w,\varphi)e^{jk_o\rho\cos w}\sin w dw \end{array} \quad (58)$$

where $\lambda(B_r)$ is the mapping of the B_r contour into the w-plane. Fig. 2 reports, in the w-plane, possible choices of Bromwich contours, *i.e.* horizontal lines $\mathrm{Im}[\eta] = \mathrm{cost}$. These contours are consistent with Figs. 13 and 14 of [36] where the properties of the two complex planes η and w are described.

Far-field components (59) are obtained applying the steepest descent path (SDP) method to equations (58):

$$E_z(\rho,\varphi) = E_z^g(\rho,\varphi) + E_z^d(\rho,\varphi) + E_z^s(\rho,\varphi) + E_z^l(\rho,\varphi) \quad (59)$$

where E_z^g is the geometrical optics (GO) contributions (see [12] for details), E_z^d the diffracted field, E_z^s the possible contributions of the surface waves, E_z^l the possible contributions of the lateral waves.

Equation (59) introduces the field E_z^s and E_z^l in the total field. These components derive from structural singularities: respectively poles and branch points of the recursive equations (53). In particular the branch points are singularities of the functions $g(w)$ and $g_1(w_1)$. The evaluation of E_z^s and E_z^l as well their interaction with the UTD contribution requires further studies. Interesting considerations on the mathematical existence of the branch line contributions as well as on the radiation conditions in the elastic wedge problems are reported in [22].

The saddle point of the function $jk_o\rho\cos w$ is $-\pi$ and the steepest descendent path is:

$$w = -\pi + gd(\mathrm{Im[w]}) + \mathrm{jIm[w]} \quad (60)$$

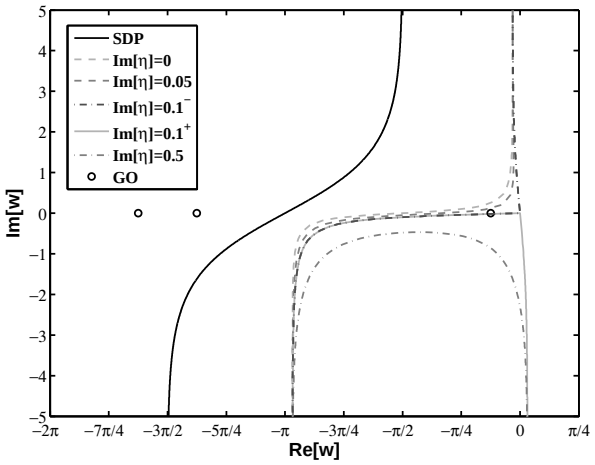

Fig. 2. Horizontal ($\mathrm{Im}[\eta] = \mathrm{cost}$.) Bromwich contours and SDP contour in the w-plane with branch points at $\pm k$ and $k = 1 - 0.1j$. The positive $\mathrm{Re}[\eta]$ direction in B_r corresponds to the direction of $\lambda(B_r)$ towards $-\pi + \arctan(-\frac{\mathrm{Im[k]}}{\mathrm{Re[k]}}) - j\infty = -3.042 - j\infty$ in the w plane.
The symbols ◯ are geometrical optics poles of the outer axial spectra referred to the test case 1 of Section V. From the left to the right side the ◯ symbols correspond respectively to the face b reflected wave, the face a reflected wave, incident wave, see also Fig. 6 of test case 1 in Section V.

where $gd(x)$ denotes the Gudermann function:

$$gd(x) = sgn(x)\arccos(1/\cosh(x)) \quad (61)$$

Fig. 2 reports the SDP contour, too. To integrate (58), the contour is deformed to the SDP passing over the saddle point $-\pi$. In order to deform the $\lambda(B_r)$ contour to the SDP, we assume B_r with $\mathrm{Im}[\eta] < \mathrm{Im}[-\mathrm{k_o}]$ where small loss assumption is considered $\mathrm{Im}[\mathrm{k_o}] \lesssim 0$. This choice also avoids the influence of the branch line cuts of the function $\xi(\eta)$ (the branch points are $\pm k_o$) on the approximated numerical solution, see Fig. 14 of [36] for details.

The contour deformation process can capture singularities of $\hat{V}_+(w,\varphi)$ as poles and branch points, located in the region between the two contours $\lambda(B_r)$ and the SDP. On the SDP the exponential argument $jk_o\rho\cos w$ is equal to $-jk_o\rho(1+jh(w))$ where $h(w)$ is a continuous real function that goes to $-\infty$ toward the end points of the path.

The total far field assumes the following form (62), where poles are related to geometrical optics fields' components (non-structural singularities) and possible surface waves (structural singularities), whereas branch points are related to lateral waves due to the $g(w)$ and $g_1(w_1)$ functions (structural singularities).

$$\begin{array}{c} E_z(\rho,\varphi) = -\frac{k_o e^{-jk_o\rho}}{2\pi}\int_{\mathrm{SDP}} \hat{V}_+(w,\varphi)e^{k_o\rho h(w)}\sin w dw + \\ -\frac{k_o}{2\pi}\int_b \hat{V}_+(w,\varphi)e^{+jk_o\rho\cos w}\sin w dw + \\ -jk_o\sum_i \mathrm{Res}[\hat{\mathrm{V}}_+(\mathrm{w},\varphi)]_{\mathrm{w_i}(\varphi)}\ \mathrm{e}^{+\mathrm{jk_o}\rho\cos\mathrm{w_i}(\varphi)}\sin\mathrm{w_i}(\varphi) \end{array} \quad (62)$$

In (62) $w_i(\varphi) = w_{oi} \pm \varphi$ are the poles of $\hat{V}_+(w,\varphi)$, w_{oi} are the poles of the axial spectral unknown $\hat{V}_+(w)$, and b is the contour deformation to consider the possible contribution of branch points w_b originated by the $g(w)$ function in the application of recursive equations.

A. Geometrical Optics fields

The contribution of geometrical optics field arises from the residues of the poles $w_i(\varphi)$ when the poles are captured by the contour deformation from $\lambda(B_r)$ to the SDP in the w-plane (see Fig. 2):

$$E_z^g(\rho,\varphi) = -jk_o \sum_i \mathrm{Res}[\hat{\mathrm{V}}_\mathrm{d}(\mathrm{w},\varphi)]_{\mathrm{w_i}(\varphi)}\ \mathrm{e}^{+\mathrm{jk_o}\rho\cos\mathrm{w_i}(\varphi)} \tag{63}$$

where $\hat{V}_d(w,\varphi) = \hat{V}_+(w,\varphi)\sin(w)$.

The number of GO poles (non-structural singularities) depends on the incident angle φ_o and the observation angle φ. For certain ranges of the two angles we can have contribution from incident plane waves, reflected plane waves, transmitted plane waves and multiple reflected/trasmitted plane waves. Besides, the poles relevant to the plane waves could be complex in presence of total reflections inside the wedge with complex trasmission/reflection coefficients. The GO terms assumes the following form:

$$e^{+jk_o\rho\cos(w_i(\varphi))} = e^{jk_o\rho\cos(w_{oi}\pm\varphi)} = e^{-jk_o\overrightarrow{\rho}\cdot\hat{k}_{oi}} \tag{64}$$

where $\hat{k}_{oi} = -\hat{x}\cos w_{oi} \pm \hat{y}\sin w_{oi}$ is the unit vector of the associated plane wave.

Let us suppose real poles $w_i(\varphi) = w_{oi} \pm \varphi$. When we vary the observation angle φ, some of the poles $w_i(\varphi)$ of $\hat{V}_+(w,\varphi)$ can cross to the left the SDP contour centered in $-\pi$. In this context these poles are not anymore captured by the contour deformation and their contributions disappear in the total field creating shadow regions for the corresponding GO waves. We recall that the w_{oi} are the poles of the axial spectrum $\hat{V}_+(w)$ for $\varphi = 0$ and $-\pi$ is the saddle point in SDP. The shadow regions are generated by the poles w_{oi} located in the interval $-\pi - \Phi < w < -\pi + \Phi$ as $-\Phi < \varphi < -\Phi$. Shadow regions are related to diffraction component to obtain continuous field passing through the shadow boundaries.

Since the Fredholm factorization provides the approximate solution of the spectra only in the strip $-\Phi \le Re[w] \le 0$, we must resort to the recursive equations (53) in order to obtain the requested spectra. We observe that the integral term in Fredholm integral equations contributes only to the diffracted fields since it does not contain any poles. Therefore we can obtain the poles and the relevant residues for the non structural poles by ignoring the integral term in the Fredholm factorization, hence it is not necessary to solve the integral equations to estimate the GO components. This property is well known in the literature as reported in [18], [21], [23]. Similar considerations can be applied for the interior region.

An excellent discussion of geometrical optics' contributions is reported in [12] where multiple reflected and transmitted waves are treated.

B. Diffracted fields

The SDP integral in (62) represents the diffracted field:

$$\begin{aligned} E_z^d(\rho,\varphi) &= -\tfrac{k_o e^{-jk_o\rho}}{2\pi}\int_{\mathrm{SDP}} \hat{V}_+(w,\varphi)e^{k_o\rho h(w)}\sin w dw = \\ &= E_o \tfrac{e^{-j(k_o\rho+\frac{\pi}{4})}}{\sqrt{2\pi k_o\rho}} D(\varphi,\varphi_o) \end{aligned} \tag{65}$$

where $D(\varphi,\varphi_o)$ is the Geometrical Theory of Diffraction (GTD) coefficient. As $k_o\rho \to \infty$, the major contribution in (65) is located near the saddle point $-\pi$ because of the exponential decay of $e^{k_o\rho h(w)}$, therefore the GTD diffraction coefficient is:

$$D(\varphi,\varphi_o) = \frac{-k_o\hat{V}_d(-\pi,\varphi)}{jE_o} \tag{66}$$

where $\hat{V}_d(w,\varphi) = \hat{V}_+(w,\varphi)\sin(w)$. The external GTD diffraction coefficient ($|\varphi| < \Phi$) assumes the explicit form (67) where $\hat{V}_d(w) = \hat{V}_+(w)\sin(w)$ is an odd function for real value of w while the plus functions $\hat{I}_+(w)$ and $\hat{V}_+(w)$ are even.

$$D(\varphi,\varphi_o) = k_o \tfrac{Z_o\left[\hat{I}_+(-\pi-\varphi)-\hat{I}_+(-\pi+\varphi)\right]+\hat{V}_d(-\pi-\varphi)+\hat{V}_d(-\pi+\varphi)}{2jE_o} \tag{67}$$

Equation (67) is consistent with the definition in terms of Sommerfeld's functions presented in [36]:

$$s_E(w) = \frac{jk_o}{2}\left[-\sin w\hat{V}_+(w) + Z_o\hat{I}_+(w)\right] \tag{68}$$

$$D(\varphi,\varphi_o) = \frac{s_E(\varphi-\pi) - s_E(\varphi+\pi)}{E_o} \tag{69}$$

Uniform expressions of the diffraction component are obtained using the Uniform Theory of Diffraction (UTD) [45]-[48]:

$$E_z^d(\rho,\varphi) = E_o\tfrac{e^{-j\left(k_o\rho+\frac{\pi}{4}\right)}}{\sqrt{2\pi k_o\rho}}C(\varphi,\varphi_o) \tag{70}$$

$$\begin{aligned} C(\varphi,\varphi_o) \quad &= \tfrac{s_E(\varphi-\pi)-s_E(\varphi+\pi)}{E_o} + \tfrac{1-F\left(2k_o\rho\cos^2\frac{\varphi-\varphi_o}{2}\right)}{2\cos\frac{\varphi-\varphi_o}{2}} + \\ &+R_a\tfrac{1-F\left(2k_o\rho\cos^2\frac{\varphi+\varphi_o-2\Phi}{2}\right)}{2\cos\frac{\varphi+\varphi_o-2\Phi}{2}} + R_b\tfrac{1-F\left(2k_o\rho\cos^2\frac{\varphi+\varphi_o+2\Phi}{2}\right)}{\cos\frac{\varphi+\varphi_o+2\Phi}{2}} + \\ &+\sum_q \Gamma_q\tfrac{1-F\left(2k_o\rho\cos^2\frac{\varphi-\varphi_q-\pi}{2}\right)}{\cos\frac{\varphi-\varphi_q-\pi}{2}} \end{aligned} \tag{71}$$

where R_a, R_b and Γ_q are the Fresnel's reflection coefficients respectively due to the first reflection on face a and b, and the q multiple trasmissions/reflections through the wedge (see also [12] for the evaluation of the coefficients). Uniform expressions are required when GO poles $w_i(\varphi)$ are near the saddle point $-\pi$. In particular we recall that shadow regions are possible for singularities of the axial spectra located in $-\pi - \Phi < w < -\pi + \Phi$. The uniform expression $E_z^g(\rho,\varphi) + E_z^d(\rho,\varphi)$ ensures the continuity when the observation angle φ crosses the shadow boundaries.

The function $F(z)$ is the Kouyoumjian-Pathak transition function defined in [47] and its application in the framework of Wiener-Hopf formulations is reported in eq. (63) of [36].

Concerning the interior region ($|\varphi_1| < \Phi_1$), we need to slightly modify the equations and the quantities involved in the definition of the diffracted field. Using the symmetry relations (56) it yields:

$$s_E^{int}(w_1) = \frac{jk_1}{2}\left[-\sin w_1\hat{V}_{\pi+}(w_1) + Z_1\hat{I}_{\pi+}(w_1)\right] \tag{72}$$

$$D^{int}(\varphi_1,\varphi_o) = \frac{s_E^{int}(-\varphi_1-\pi) - s_E^{int}(-\varphi_1+\pi)}{E_o} \tag{73}$$

with explicit expression reported in (74).

$$D^{int}(\varphi_1,\varphi_o)=k_1\frac{Z_1[\hat{I}_{\pi+}(\varphi_1-\pi)-\hat{I}_{\pi+}(-\pi-\varphi_1)]+\hat{V}_{\pi d}(\varphi_1-\pi)+\hat{V}_{\pi d}(-\pi-\varphi_1)}{2jE_o} \tag{74}$$

As for the exterior region, uniform expressions $C^{int}(\varphi_1,\varphi_o)$ are required when GO poles $w_{1i}(\varphi_1) = -\varphi_1 \pm w_{1io}$ (with w_{1io} poles of the axial spectra $\hat{V}_{\pi+}(w_1)$ and $\hat{I}_{\pi+}(w_1)$) are near the saddle point $-\pi$: shadow region are possible for poles in $-\pi-\Phi_1 < w_1 < -\pi+\Phi_1$. Consequently uniform expressions of the diffracted field (75) are of the same kind of the one for exterior region (70) and $E_z^g(\rho,\varphi)+E_z^d(\rho,\varphi)$ is continuous when it crosses the shadow boundaries inside (as outside) the dielectric wedge.

$$E_z^d(\rho,\varphi_1)=E_o\frac{e^{-j\left(k_1\rho+\frac{\pi}{4}\right)}}{\sqrt{2\pi k_1\rho}}C^{int}(\varphi_1,\varphi_o) \tag{75}$$

The complete GTD diffraction coefficient is defined by:

$$D^{tot}(\varphi,\varphi_o)=\begin{cases} D(\varphi,\varphi_o) & |\varphi|<\Phi \\ D^{int}(\pi-\varphi,\varphi_o) & \Phi<\varphi<\pi \\ D^{int}(-\pi-\varphi,\varphi_o) & -\pi<\varphi<-\Phi \end{cases} \tag{76}$$

Note that the complete UTD diffraction coefficient $C^{tot}(\varphi,\varphi_o)$ assumes the same form of $D^{tot}(\varphi,\varphi_o)$.

V. Validation and Numerical results

The efficiency, the convergence and the validation of the proposed approximate solutions is illustrated through several test problems. The quantities used in this section are explicitly defined in the previous section: Far-field evaluation. Some of the following numerical results and figures show the comparison between the solution of the dielectric wedge test case and the solution of the perfect conducting (PEC) wedge with the rest of physical parameters unchanged.

The first test case is investigated in detail, reporting the whole procedure to solve the problem: from the definition of Wiener-Hopf spectral unknowns to the evaluation of the total field. Moreover, the test cases show the convergence properties of the proposed method and some physical properties of the diffraction by a dielectric wedge. The last test compares our solution with the one of [12]-[13] and shows the computational efficiency of our method. The first three tests consider non-standard plus unknowns while the fourth non-standard minus unknowns.

All the test cases make reference to Fig. 1. In particular, the wedge is illuminated by a plane wave impinging from a direction φ_o (leaving the wedge with direction $\varphi_I=\varphi_o-\pi$), see (77). In this paper we denote the azimuthal direction of the GO waves with φ_{lab} where the subscripts lab are in upper case (lower case) if referred to a wave that leaves (approaches) the wedge: for instance, the face a reflected wave propagates as $e^{jk_o\rho\cos(\varphi-\varphi_{ra})}=e^{-jk_o\rho\cos(\varphi-\varphi_{RA})}$ with $\varphi_{ra}=2\Phi-\varphi_o$ and $\varphi_{RA}=\varphi_{ra}-\pi$, see Fig. 1.

A. Test case 1

The first test case analyzes all the properties of our solution in terms of spectral quantities, diffraction coefficients, total fields. With reference to Fig. 1 the physical parameters of the problem are: $\Phi=3\pi/4$, $\varepsilon_r=3$, $\varphi_o=\pi/8$, $\delta=\pi/2$ and $|E^i|=1V/m$.

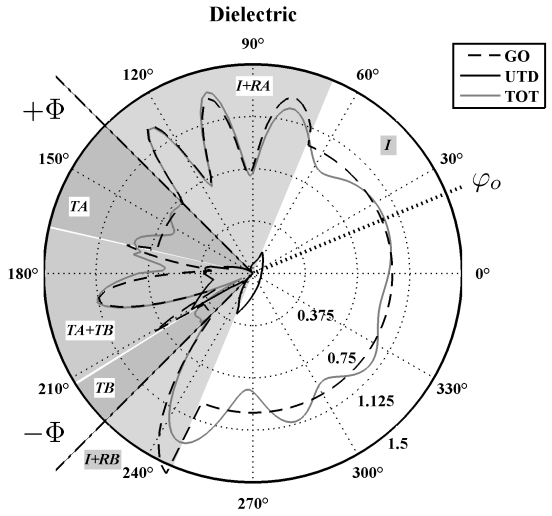

Fig. 3. Test case 1: the GO field, the UTD component and, the total far-field pattern at $k\rho=10$.

According to GO, the E-polarized incident plane wave impinges on the dielectric wedge and generates two reflected waves and two transmitted waves. The two transmitted wave are not reflected in the interior region.

This configuration allows to define four geometrical optics shadow boundaries: face a reflected shadow boundary, face b reflected shadow boundary, face a transmitted shadow boundary and, face b transmitted shadow boundary. No incident shadow boundary exists. As shown in Fig. 3 with different gray color backgrounds, there are six GO regions: incident wave region $\varphi_{RB}<\varphi<\varphi_{RA}$ (I), incident and face a reflected waves region $\varphi_{RA}<\varphi<\Phi$ (I+RA), incident and face b reflected waves region $-\Phi<\varphi<\varphi_{RB}$ (I+RB), face a transmitted wave region $\Phi<\varphi<\varphi_{TA}$ (TA), face b transmitted wave region $\varphi_{TB}<\varphi<-\Phi$ (TB) and, face a and b transmitted waves region $(-\pi<\varphi<\varphi_{TB})\bigcup(\varphi_{TA}<\varphi<\pi)$ (TA+TB).

Fig. 3 reports the GO field, the UTD component and, the total far-field at the distance $k\rho=10$ from the edge of the wedge. According to GO, the problem under examination shows:

- a face a reflected wave angle $\varphi_{RA}=-\pi-\varphi_o+2\Phi=3\pi/8\simeq 1.18_{rad}=67.6^o$
- a face b reflected wave angle $\varphi_{RB}=\pi-\varphi_o-2\Phi=-5\pi/8\simeq -1.96_{rad}=-112.3^o$
- a face a transmitted wave angle $\varphi_{TA}=-2\pi+\Phi+\arccos(\frac{\cos(\varphi_o+\Phi_1)}{\sqrt{\varepsilon_r}})\simeq -2.58_{rad}=-147.8^o$
- a face b transmitted wave angle $\varphi_{TB}=-2\pi-\Phi-\arccos(\frac{\cos(-\varphi_o+\Phi_1)}{\sqrt{\varepsilon_r}})\simeq 2.92_{rad}=167.3^o$

The solution of the problem is obtained applying the discretization method reported in Section III where the Fredholm factorization method is applied to the GWHE with discretization parameters $A=10$, $h=0.05$.

Fig. 4 shows the behavior of the numerical solution in terms of the spectral unknowns $\hat{V}_+(w)$ and $\hat{I}_+(w)$ in the regularity segment $-\Phi\le w\le 0$: the outer axial starting spectra (as defined in Section III) is purely imaginary (Appendix III). Relative errors are reported in $\log_{10}$ scale by considering as

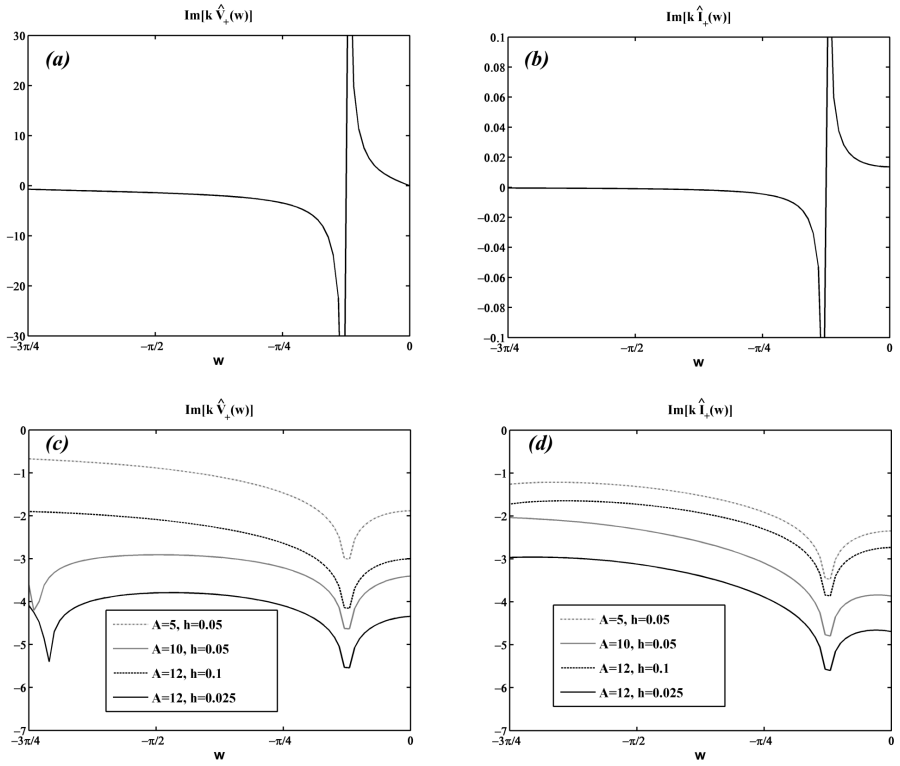

Fig. 4. Test case 1: a-b) Imaginary parts of spectral unknowns $\hat{V}_+(w)$ and $\hat{I}_+(w)$ in the regularity segment $-\Phi \leq w \leq 0$; c-d) relative error in $\log_{10}$ scale of $Im[k\hat{V}_+(w)]$ and $Im[k\hat{I}_+(w)]$: the reference solution is obtained with discretization parameters $A = 12,\ h = 0.015$.

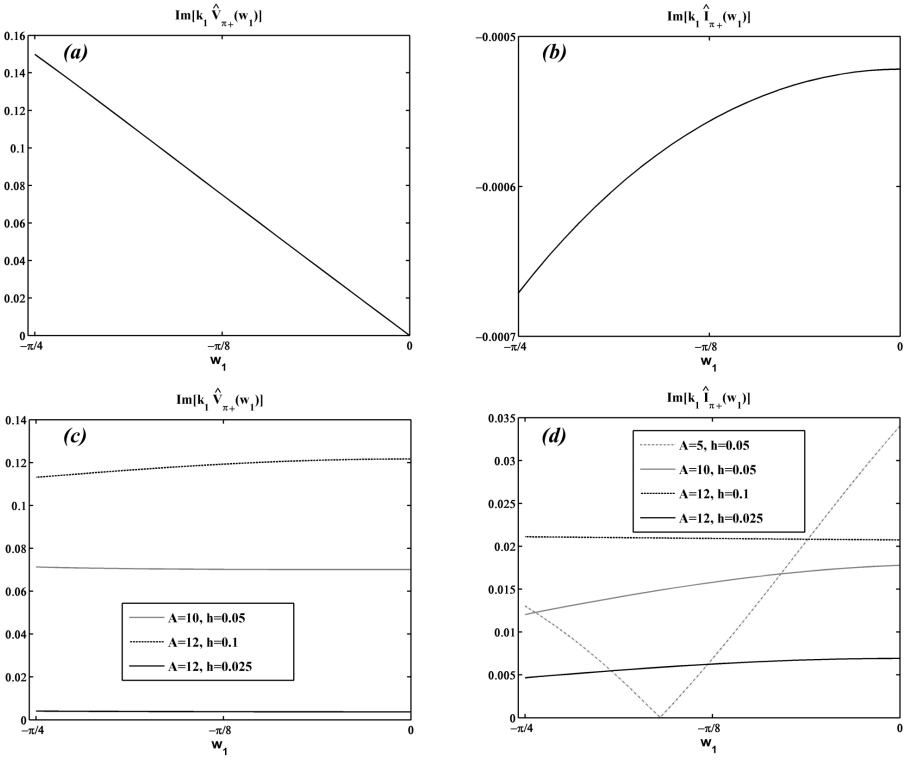

Fig. 5. Test case 1: a-b) Imaginary parts of spectral unknowns $\hat{V}_{\pi+}(w_1)$ and $\hat{I}_{\pi+}(w_1)$ in the regularity segment $-\Phi_1 \leq w_1 \leq 0$; c-d) relative error in linear scale of $Im[k_1\hat{V}_{\pi+}(w_1)]$ and $Im[k_1\hat{I}_{\pi+}(w_1)]$: the reference solution is obtained with discretization parameters $A = 12,\ h = 0.015$.

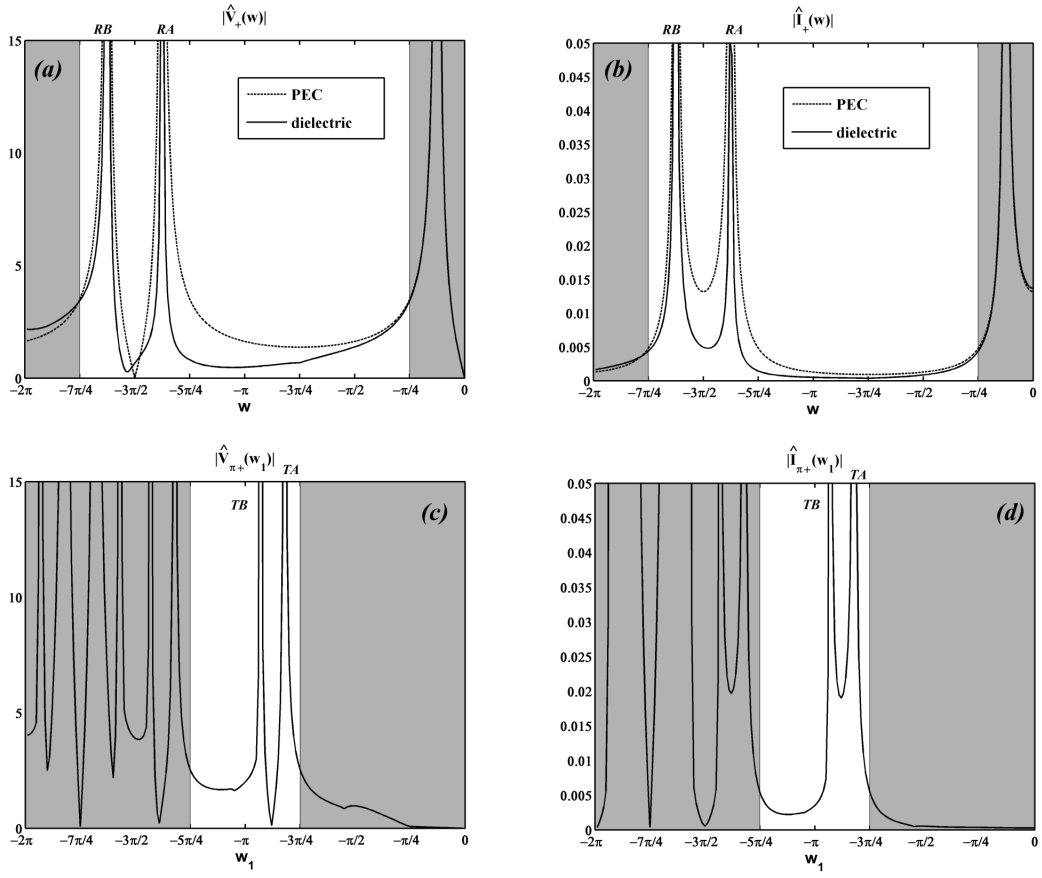

Fig. 6. Test case 1: a-d) Absolute value of the spectral unknowns $\hat{V}_+(w)$, $\hat{I}_+(w)$, $\hat{V}_{\pi+}(w_1)$ and $\hat{I}_{\pi+}(w_1)$ in $(-2\pi, 0)$. Dark gray regions are not used to evaluate the GTD coefficients.

reference solution the one obtained for discretization parameters $A = 12,\ h = 0.015$. For the numerical solution we have chosen different values of the integration parameter A and h in order to confirm the convergence of our technique. However, an excessive value of A ($A > 15$) yields ill-conditioned matrices in the discretization process.

Fig. 5 shows the behavior of the numerical solution in terms of the spectral unknowns $\hat{V}_{\pi+}(w_1)$ and $\hat{I}_{\pi+}(w_1)$ in the regularity segment $-\Phi_1 \leq w_1 \leq 0$.

As reported in Section IV the evaluation of the GTD coefficients requires the analytic continuation of the spectral unknowns $\{\hat{V}_+(w), \hat{I}_+(w)\}$ and $\{\hat{V}_{\pi+}(w_1), \hat{I}_{\pi+}(w_1)\}$ respectively in the interval $-\pi - \Phi < w < -\pi + \Phi$ and $-\pi - \Phi_1 < w_1 < -\pi + \Phi_1$. The required analytical continuation is obtained through the recursive equations reported in (53).

Fig. 6 shows the behavior of the absolute value of the spectral unknowns $\{\hat{V}_+(w), \hat{I}_+(w)\}$ and $\{\hat{V}_{\pi+}(w_1), \hat{I}_{\pi+}(w_1)\}$. The figure highlights the spectral regions necessary to evaluate the GTD diffraction coefficients (67) and (74), *i.e.* $-\pi - \Phi < w < -\pi + \Phi$ and $-\pi - \Phi_1 < w_1 < -\pi + \Phi_1$. The figure shows also the GO poles relevant to the GTD for test case 1. In particular $\{\hat{V}_+(w), \hat{I}_+(w)\}$ show peaks for the reflected waves, while $\{\hat{V}_{\pi+}(w_1), \hat{I}_{\pi+}(w_1)\}$ for the transmitted waves. The location of the poles agrees with the standard GO theory, for instance consider $w_{RA} \simeq -4.32$ and $w_{TB} \simeq -2.92$: using equations (67) and (74) and, considering that the spectral unknowns are even function in w (w_1), we obtain that $\varphi_{RA} = -w_{RA} - \pi \simeq 1.18rad$ and $\varphi_{TB} = -w_{TB} \simeq 2.92rad$ (since $\varphi_1 = \pi - \varphi$). Similar considerations hold for the other GO poles. The GO components can be obtained by using standard techniques or by applying (63). Notice that the study of the axial spectra is fundamental. In fact, if w_{oi} is a singularity of $\hat{V}_+(w)$ ($\hat{I}_+(w)$), the spectrum of $\hat{V}_+(w, \varphi)$ ($\hat{I}_+(w, \varphi)$) presents the singularities $w_{oi} \pm \varphi$ that can be captured by the integration contour deformation from B_r to SDP, see subsection IV-A. The singularities of $\hat{V}_+(w)$ ($\hat{I}_+(w)$) are reported in Fig. 2 together with different integration contours. While $k\hat{V}_+(w)$ and $k\hat{I}_+(w)$ are almost purely imaginary functions in $(-2\pi, 0)$ (purely imaginary in $(-\Phi, 0)$, see Appendix III); $k_1\hat{V}_{\pi+}(w_1)$ and $k_1\hat{I}_{\pi+}(w_1))$ are complex functions as shown in Fig. 7, where for the sake of simplicity we have reported only the voltage spectra. The approximate total GTD diffraction coefficients are estimated substituting the approximations of the spectral unknowns in (67) and (74). Fig. 8.a reports the absolute value of the total GTD diffraction coefficient (in dB) for each observation angle φ. The peaks of the GTD diffraction coefficients occur for the GO angles: reflected and transmitted waves. The convergence is shown in Fig.8.b for different integration parameters through the evaluation of the relative error in $\log_{10}$ scale with respect to the reference solution

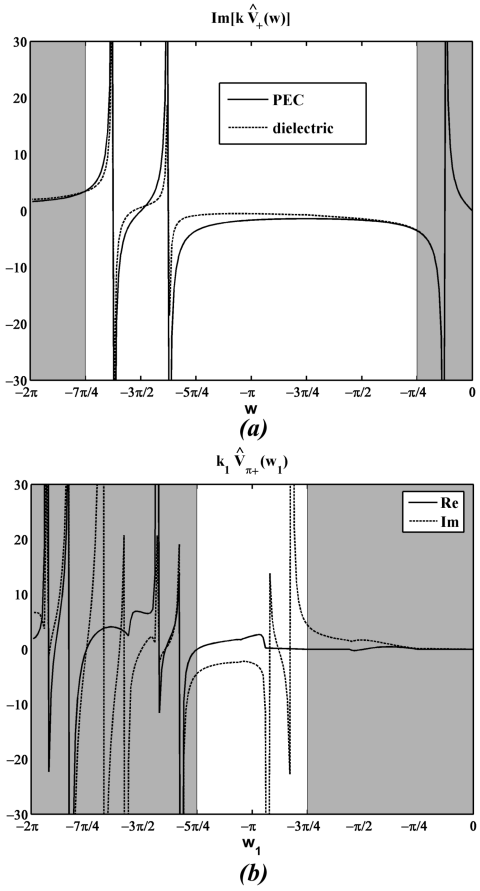

Fig. 7. a) $Im[k\hat{V}_+(w)]$ for the test case 1 and the PEC wedge, b) real and imaginary part of $k_1\hat{V}_{\pi+}(w_1)$.

obtained for $A = 12$, $h = 0.015$. The $\log_{10}$ scale measures the level of precision in term of digits for each observation angle φ. Fig. 8.c reports the phase of the total GTD diffraction coefficient (in dB) for each observation angle φ. Figs. 8.a and 8.c show also the plots for the PEC wedge.

The complete solution is reported in Figs. 9 and 10. The first figure reports the total field, GO field component, UTD field component at the distance $k\rho = 10$. Gray regions are inside the wedge. The second figure shows the comparison between the total field of the dielectric wedge with the one of the PEC wedge. We notice that Fig. 9 shows a small loss of convergence for $\varphi \simeq +2.97$ and $\varphi \simeq -2.36$: the reasons for the *corner* behavior are different.

In the first case, when $\varphi \simeq +2.97$, the problem is due to the spectral reconstruction of the Wiener-Hopf π unknowns in w_1, *i.e.* $\hat{V}_{\pi+}(w_1)$ and $\hat{I}_{\pi+}(w_1)$. In fact, for $\varphi \simeq +2.97$ the UTD/GTD field component is related to the evaluation of $\hat{V}_{\pi+}(w_1)$ and $\hat{I}_{\pi+}(w_1)$ in $w_1 = -2.97$, see (76) and (74). We recall that the recursive equations are used to estimate the spectral unknowns out of the regularity strips ($-\Phi \leq \mathrm{Re}[w] \leq 0$ and $-\Phi_1 \leq \mathrm{Re}[w_1] \leq 0$) in particular in the GTD intervals ($-\pi-\Phi < w < -\pi+\Phi$ and $-\pi-\Phi_1 < w_1 < -\pi+\Phi_1$). Fig. 11 shows the mapping used in the estimation of π functions out of the regularity segment $-\Phi_1 \leq w_1 \leq 0$ for real value of w_1 (see (53)), *i.e.* $w = \Phi + g_1(w_1+\Phi_1)$. The map starts from $w_1 = -\Phi_1$ that yields $w = \Phi - \arccos(\sqrt{\varepsilon_r}) \simeq 3\pi/4 - j1.1462$ and goes all over the gray line as long as $w_1 = -\pi-\Phi_1$ is mapped

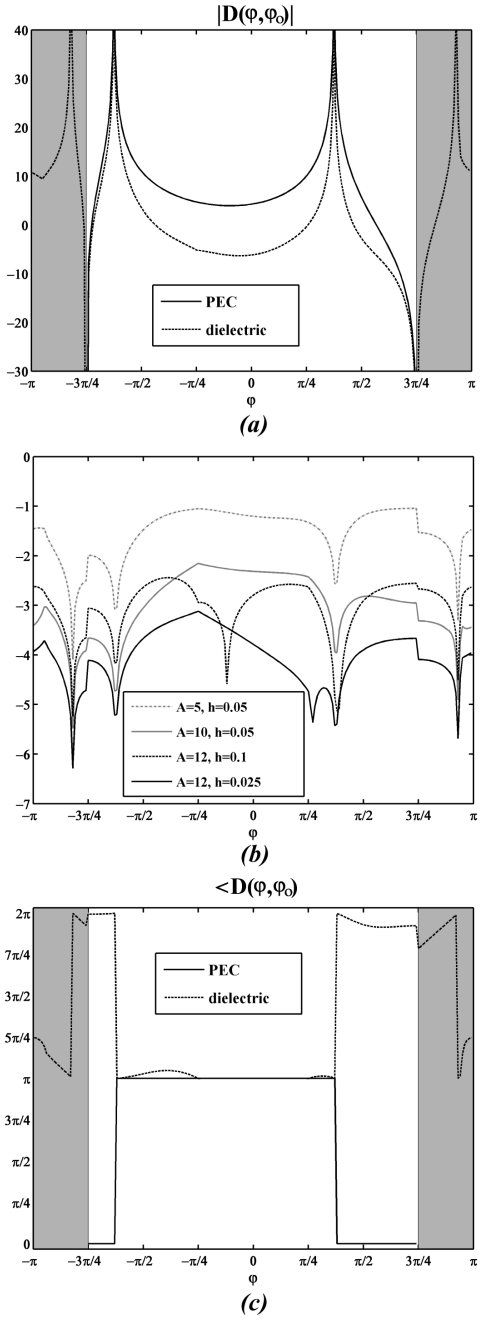

Fig. 8. Test case 1: a) absolute value of the total GTD diffraction coefficient (dB), b) GTD diffraction's relative error in $\log_{10}$ scale using different set of integration parameters (reference solution $A = 12$, $h = 0.015$), c) phase of the total GTD diffraction coefficient.

into $w = -\Phi_1 + \arccos(\sqrt{\varepsilon_r}) \simeq -\pi/4 + j1.1462$. Uniform sampling for real w_1 is mapped into non-uniform sampling in complex w. In particular the significant point $w_1 = -2.97$ is mapped into $w = -\Phi_1$ where the mapping shows a change in slope and highly non uniform sampling. This is the cause for the loss of convergence in UTD/GTD for $\varphi \simeq +2.97$.

The second direction where we experience loss of convergence is $\varphi \simeq -2.36$ and it is due to the UTD uniform expression of the GTD field component. Since $\varphi \simeq -2.36$ is very close to the interface between the two materials ($\varphi = -\Phi$), the Kouyoumjian-Pathak (KP) transition function [47] is not adequate to model the problem: the uniform diffraction

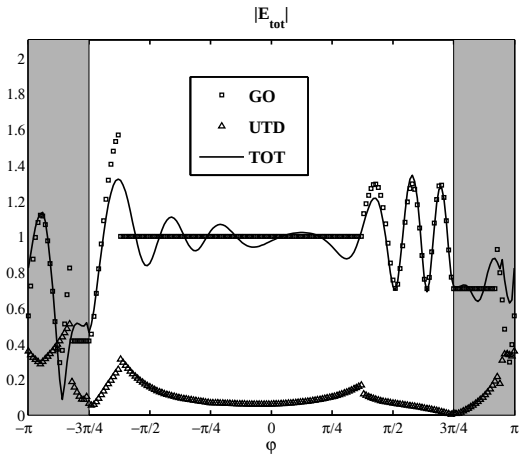

Fig. 9. Test case 1: Total field (solid line), GO field component (squares), UTD field component (triangles) at $k\rho = 10$.

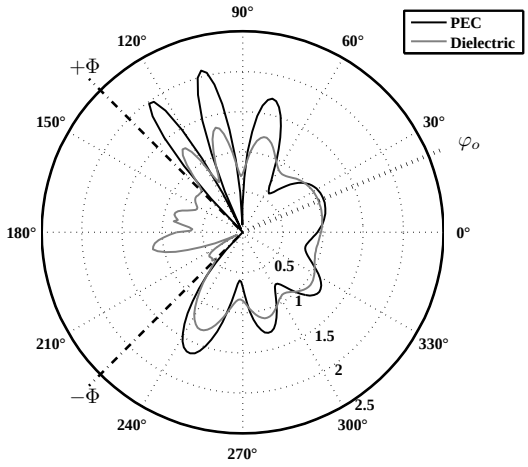

Fig. 10. Test case 1: comparison between the total field of the dielectric (gray line) and the PEC wedge (black line)at $k\rho = 10$.

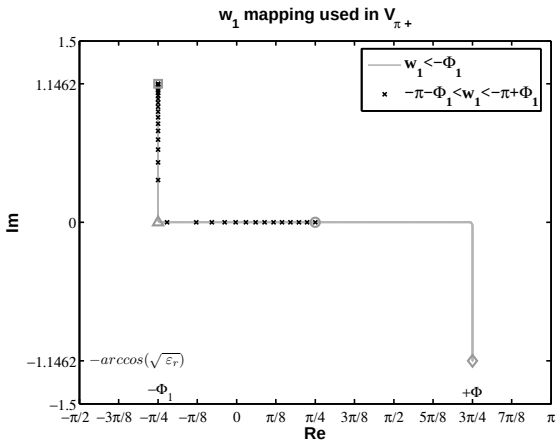

Fig. 11. Test case 1: $w = \Phi + g_1(w_1 + \Phi_1)$ mapping used in the estimation of π functions out of the regularity segment $-\Phi_1 \leq w_1 \leq 0$. The map starts from $w_1 = -\Phi_1$ that yields $w = \Phi - \arccos(\sqrt{\varepsilon_r})$ ($\arccos(\sqrt{\varepsilon_r}) \simeq j1.1462$) and goes all over the gray line as long as $w_1 = -\pi - \Phi_1$ is mapped into $w = -\Phi_1 + \arccos(\sqrt{\varepsilon_r})$. Uniform sampling for real w_1 corresponds to non-uniform sampling in complex w. The symbols $\diamondsuit, \bigcirc, \triangle, \square$ respectively are the mapped value of $w_1 = -\Phi_1, \Phi_1 - \pi, -\Phi_1 - \arccos(-\frac{1}{\sqrt{\varepsilon_r}}), -\pi - \Phi_1$.

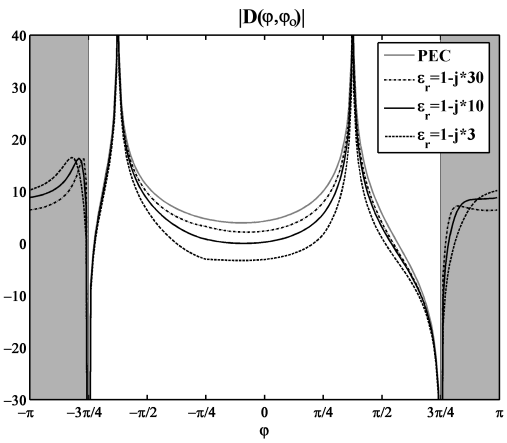

Fig. 12. Test case 2: the GTD diffraction coefficient (dB).

component is a cylindrical wave whose intensity should vanish at the interface, on the contrary, at first sight, the KP transition function's slope does not consider the change of materials.

B. Test case 2

The second test case shows the convergence properties of our solution in terms of GTD diffraction coefficient. The closed form solution of the PEC wedge, see for example [36], allows to compare the dielectric wedge solution when the relative permittivity is with high imaginary part and real part equal to 1. Fig. 12 shows the GTD diffraction coefficient (in dB) when $\Phi = 3\pi/4$, $\varepsilon_r = 1 - j\varepsilon_i$, $\varphi_o = \pi/8$, $\delta = \pi/2$ and $|E^i| = 1V/m$ with discretization parameters $A = 10$, $h = 0.05$. By increasing ε_i the solution converges to the PEC wedge.

C. Test case 3

The third test case highlights the capabilities of our method to model the scattering and diffraction by a dielectric wedge in presence of multiple reflections and transmissions. With reference to Fig. 1 the physical parameters of the problem are: $\Phi = 7\pi/8$, $\varepsilon_r = 3$, $\varphi_o = 13\pi/32$, $\delta = \pi/2$ and $|E^i| = 1V/m$.

The E-polarized incident plane wave impinges on the dielectric wedge and generates one face a reflected wave and one face a transmitted wave. The transmitted wave is totally reflected inside the wedge for two times and generates two evanescent transmitted waves through the two interfaces. This configuration allows to define three geometrical optics shadow boundaries (omitting the ones for the evanescent waves): incident shadow boundary, face a reflected shadow boundary, face a transmitted and double totally reflected shadow boundary. As a consequence, there are five GO regions:

- region 1: incident wave
- region 2: incident wave, face a reflected wave, evanescent wave through face a
- region 3: face a transmitted wave, face b reflected wave from face a transmitted wave, double reflected wave from face a transmitted wave
- region 4: face a transmitted wave, face b reflected wave from face a transmitted wave
- region 5: evanescent wave through face b

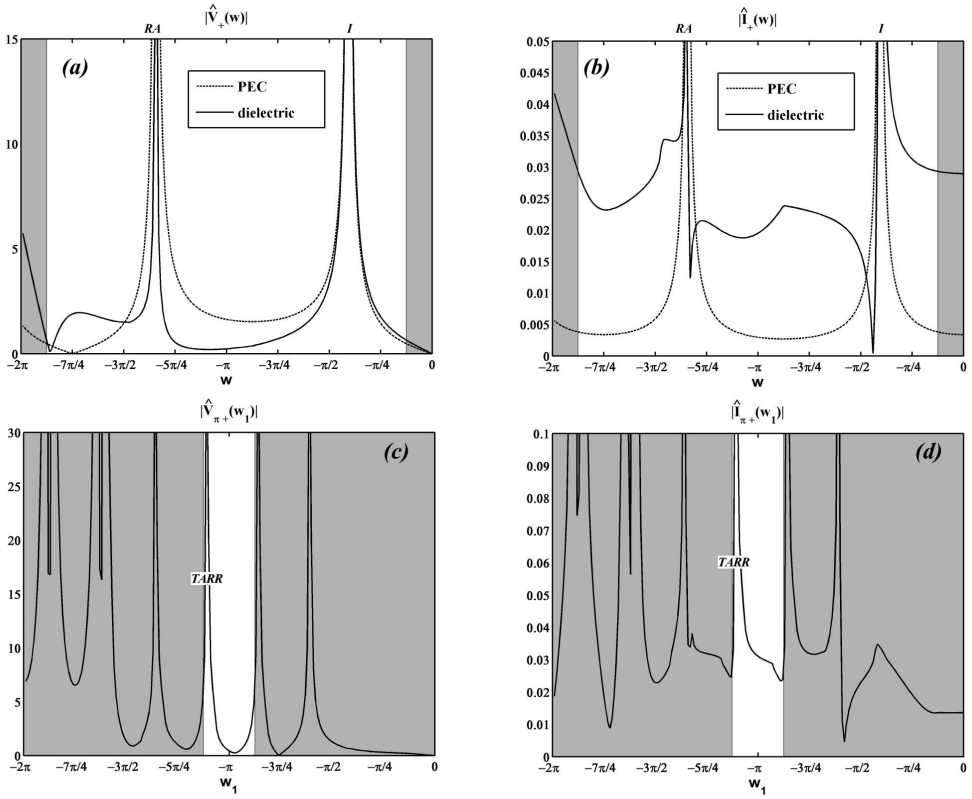

Fig. 14. Test case 3: a-d) absolute value of the spectral unknowns $\hat{V}_+(w)$, $\hat{I}_+(w)$, $\hat{V}_{\pi+}(w_1)$ and $\hat{I}_{\pi+}(w_1)$ in $(-2\pi, 0)$. Dark gray regions are not used to evaluate the GTD coefficients.

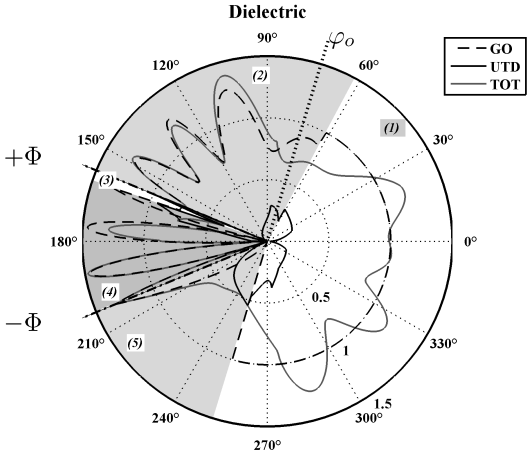

Fig. 13. Test case 3: the GO field, the UTD component and, the total far-field pattern at $k\rho = 10$.

The GO field, the UTD component and, the total far-field pattern are reported in Fig. 13 at the distance $k\rho = 10$ from the edge of the wedge.

The solution of the problem is obtained applying the discretized method reported in Section III where the Fredholm factorization method is applied to the GWHE with discretization parameters $A = 10$, $h = 0.05$. Fig. 14 shows the behavior of the absolute value of the spectral unknowns $(\hat{V}_+(w), \hat{I}_+(w))$ and $(\hat{V}_{\pi+}(w_1), \hat{I}_{\pi+}(w_1))$. The figure highlights the spectral regions necessary to evaluate the GTD diffraction coefficients (67) and (74), *i.e.* $-\pi - \Phi < w < -\pi + \Phi$ and $-\pi - \Phi_1 < w_1 < -\pi + \Phi_1$. The figure shows also the GO poles relevant to the GTD for test case 3. In particular $(\hat{V}_+(w), \hat{I}_+(w))$ show peaks for the face a reflected wave (RA) and incident wave (I), while $(\hat{V}_{\pi+}(w_1), \hat{I}_{\pi+}(w_1))$ for the transmitted and double reflected wave (TARR). Notice that the lobes reported in Figs. 14.a and 14.b are related to evanescent waves (complex poles in w).

The complete solution is reported in Figs. 15 where the total field, GO field component, UTD field component are evaluated at the distance $k\rho = 10$. Gray regions are inside the wedge. Comparison between the complete solution of the dielectric wedge with the one obtained with PEC wedge is also shown.

Note that Fig. 15.a shows loss of convergence in the diffracted component for $\varphi \approx \pm 1.475 rad$. This spurious local *corner* behavior of the solution is due to the effect of the mapping $w = \Phi + g_1(w_1 + \Phi_1)$ in the spectral reconstruction of the WH unknowns $(\hat{V}_+(w), \hat{I}_+(w))$ through the recursive equations (53) as already discussed for the WH π unknowns $(\hat{V}_{\pi+}(w_1), \hat{I}_{\pi+}(w_1))$ at the end of test case 1.

D. Test case 4

The fourth test case shows the validation of our method through the comparison of our solution with the one proposed in [12]-[13]. In this test case we shows the capabilities of our method to model the scattering and diffraction by a dielectric wedge in presence of multiple reflections and transmissions and, the performance in terms of computational time. With

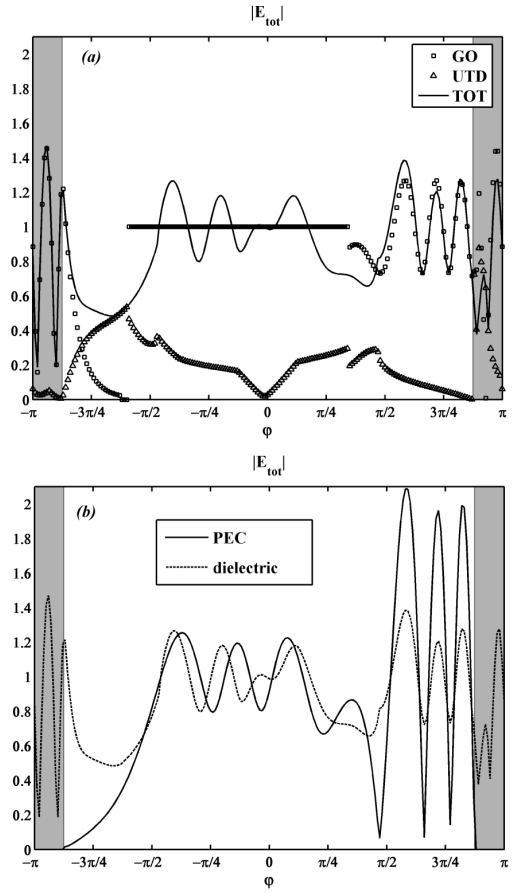

Fig. 15. Test case 3: a) Total field (solid line), GO field component (squares), UTD field component (triangles) at $k\rho = 10$, b) total field for the dielectric and PEC wedge.

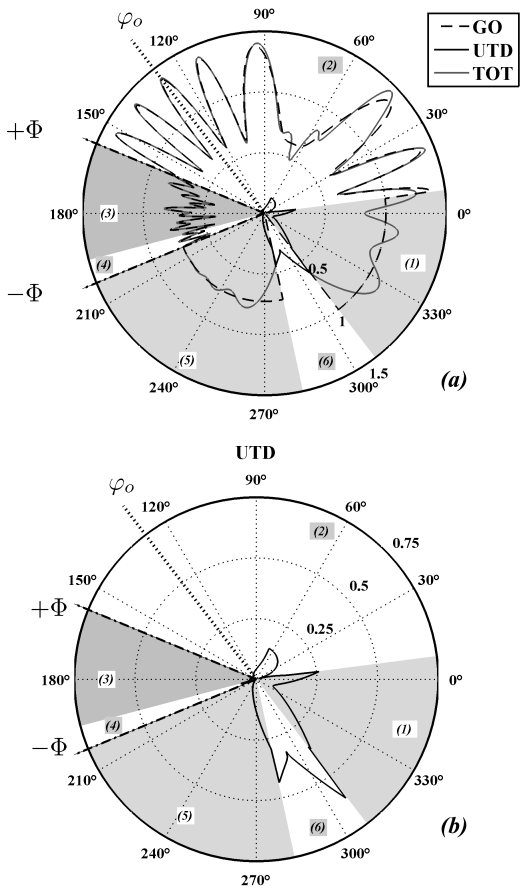

Fig. 16. Test case 4: a) the GO field, the UTD component and, the total far-field pattern at $k\rho = 10\pi$, b) the UTD component at $k\rho = 10\pi$.

reference to Fig. 1 the physical parameters of the problem are: $\Phi = 7\pi/8$, $\varepsilon_r = 2$, $\varphi_o = 17\pi/24$, $\delta = \pi/2$ and $|E^i| = 1V/m$. The E-polarized incident plane wave impinges on the dielectric wedge and generates one face a reflected wave and one face a transmitted wave. The transmitted wave is reflected and transmitted through face b. The reflected part is then totally reflected on face a and generates an evanescent transmitted wave. This configuration allows to define four geometrical optics shadow boundaries (omitting the one for the evanescent wave): incident shadow boundary, face a reflected shadow boundary, double transmitted shadow boundary, transmitted-double reflected shadow boundary. As a consequence, there are six GO regions:

- region 1: incident wave
- region 2: incident wave, face a reflected wave, evanescent wave through face a
- region 3: face a transmitted wave, face b reflected wave from face a transmitted wave, double-reflected wave from face a transmitted wave
- region 4: face a transmitted wave, face b reflected wave from face a transmitted wave
- region 5: double transmitted wave through face a and b
- region 6: no GO components

The GO field, the UTD component and, the total far-field pattern are reported in Fig. 16 at the distance $k\rho = 10\pi$ from the edge of the wedge. The figure is obtained using the Fredholm factorization method with discretization parameters $A = 10$, $h = 0.05$ and the results can easily be compared with the figures reported in [12]-[13].

Note that near $\varphi = \pi/3$ the Fig. 16.b shows a *corner* behavior due to the use of g_1 in the recursive equations (53).

Table III shows the computational speed of our implementation in Mathematica© on an Intel®Core^{TM}2 Duo CPU (P8400@2.26GHz 3GB RAM). Note that the use of Mathematica© let us handle and verify all the mathematical details of the procedure. The use of a full numerical implementation of our method would speed up the entire evaluation.

TABLE III
COMPUTATIONAL SPEED

Time	Action
< 1s	Mathematica definitions
$\lesssim 130$s	Discretization
< 2s	Linear system generation
< 5s	Linear system solution
0.01-0.03s	Spectral sample in regularity segment
0.1-0.5s	Sample of total field

VI. CONCLUSION

In this paper we present a new method to study the diffraction by an isotropic penetrable wedge using the WH technique. The solution is presented in terms of GTD diffraction coefficients, UTD diffraction coefficients and total fields.

Further work will be focused on the study of the contribution of the structural singularities and on the computational aspects for the general skew incidence case.

APPENDIX I
SOURCE TERM

This appendix is devoted to study the source term $\bar{n}_i(\alpha)$ (first-order pole function) of the Fredholm integral equation formulation (19) when the isotropic penetrable wedge is illuminated by a general plane wave at skew incidence from the outer region.

Without loss of generality, let us consider an E-polarized plane wave. The GO field of the outer region can be evaluated by solving the simple problem of reflection/transmission of plane waves at skew incidence:

$$\begin{aligned} E_z^g = e^{-j\gamma_o z}[&E_o u(\pi-|\varphi-\varphi_o|)e^{j\tau_o\,\rho\cos(\varphi-\varphi_o)}+\\ &+u(\pi-|\varphi+\varphi_o-2\Phi|)E_{or}^{(a)}e^{j\tau_o\,\rho\cos(\varphi+\varphi_o-2\Phi)}+\\ &+u(\pi-|\varphi+\varphi_o+2\Phi|)E_{or}^{(b)}e^{j\tau_o\,\rho\cos(\varphi+\varphi_o+2\Phi)}]+E_{zt}^g \end{aligned} \tag{77}$$

where $u(x)$ is the unit step function, $E_{or}^{(a,b)}$ are the reflection coefficient of the two faces a and b and, E_{zt}^g is the field re-transmitted from inside the wedge (see [12] for a deep discussion), when it is present.

In order to establish the source term $\bar{n}_i(\alpha)$ we have identified the following strategy based on engineering and mathematical considerations:
A) assuming that the GO is valid, $\bar{n}_i(\alpha)$ derives from the Laplace transform of the known GO field for $\varphi = 0, +\Phi, -\Phi$ respectively in the complex planes η, $-m$ and $-m$,
B) we evaluate the source term $\bar{n}_i(\alpha)$ using the residue theorem applied to the non-standard spectral unknowns (see Section II for definitions) *only* for the singularities located in the proper sheet of the α complex plane that contains the segment $-\Phi \le w \le 0$, see [36].

In the following we consider the case of incidence $0 < \varphi_o < +\Phi$, the opposite case $-\Phi < \varphi_o < 0$ is obtained using symmetry.

By ignoring in a first moment the existence domain of the GO components (77), the application of the η Laplace transform (3) to (77) for $\varphi = 0$ yields several first-order pole terms with poles: $\eta_o = -\tau_o \cos\varphi_o$ for the incident wave, $\eta_{ao} = -\tau_o\cos(2\Phi-\varphi_o)$ for the face a reflected wave, $\eta_{bo} = -\tau_o\cos(2\Phi+\varphi_o)$ for the face b reflected wave and η_{tn} for the n re-transmitted waves. The first three poles have the same representation in the α-plane: $\alpha_o = -\tau_o\cos\left(\frac{\pi}{\Phi}\varphi_o\right)$.

By ignoring in a first moment the existence domain of the GO components (77), the application of the $-m$ Laplace transform (3) to (77) for $\varphi = +\Phi$ yields several first-order pole terms with poles: $m_o^{(+\Phi)} = \tau_o\cos(\Phi-\varphi_o)$ for the incident wave, $m_{ao}^{(+\Phi)} = \tau_o\cos(\Phi-(2\Phi-\varphi_o)) = \tau_o\cos(-\Phi+\varphi_o)$ for the face a reflected wave, $m_{bo}^{(+\Phi)} = \tau_o\cos(\Phi-(-2\Phi-\varphi_o)) = \tau_o\cos(3\Phi+\varphi_o)$ for the face b reflected wave and $m_{tn}^{(+\Phi)}$ for the n re-transmitted waves. Note that the first two poles have the same representation in the m-plane $m_o^{(+\Phi)} = m_{ao}^{(+\Phi)}$ and through (15) we obtain that the first three $m^{(+\Phi)}$ poles have the same representation in the α-plane: $\alpha_o = -\tau_o\cos\left(\frac{\pi}{\Phi}\varphi_o\right)$.

Similar considerations hold for the third case, *i.e.* the face b $\varphi = -\Phi$: $m_o^{(-\Phi)} = \tau_o\cos(-\Phi-\varphi_o)$, $m_{ao}^{(-\Phi)} = \tau_o\cos(-3\Phi+\varphi_o)$, $m_{bo}^{(-\Phi)} = \tau_o\cos(\Phi+\varphi_o)$, and $m_{tn}^{(-\Phi)}$ respectively for the incident, the face a reflected, the face b reflected and the n re-transmitted waves. In this case $m_o^{(-\Phi)} = m_{bo}^{(-\Phi)}$ and the first three $m^{(-\Phi)}$ poles have the same representation $\alpha_o = -\tau_o\cos\left(\frac{\pi}{\Phi}\varphi_o\right)$.

We denote with $\alpha_{tn}^{(\varphi)}$ the poles of the re-transmitted waves in the α complex planes for observation angles $\varphi = 0, +\Phi, -\Phi$. These poles are obtained using the first relation of (13) for $\varphi = 0$ and (15) for $\varphi = +\Phi, -\Phi$.

We assert that the source term $\bar{n}_i(\alpha)$ is obtained through the residue theorem applied to the non-standard spectral unknowns only for the singularities located in the proper sheet of the α complex plane that contains the segment $-\Phi \le w \le 0$ [36].

Although the spectral unknowns in the α complex plane present the poles α_o and $\alpha_{tn}^{(\varphi)}$, we consider only the contribution of α_o since: either 1) $\alpha_{tn}^{(\varphi)}$ is associated to a re-transmitted wave with existence domain that excludes $\varphi = 0, +\Phi, -\Phi$ directions or 2) $\alpha_{tn}^{(\varphi)}$ is located in the improper sheet of the α plane for $\varphi = 0, +\Phi, -\Phi$ or 3) both the previous conditions are simultaneously satisfied. The second condition is easily verified using the w-plane: the condition becomes $-\Phi \le w_{tn}^{(\varphi)} \le 0$ with real $w_{tn}^{(\varphi)}$ for $\varphi = 0, +\Phi, -\Phi$ where $w_{tn}^{(\varphi)}$ corresponds to $\alpha_{tn}^{(\varphi)}$ using the expressions of η and m in w, see (22)-(23).

Starting from (14) we extract the source term related to the source pole $\alpha_o = -\tau_o\cos\left(\frac{\pi}{\Phi}\varphi_o\right)$ from the non-standard unknowns. The location of α_o in the α complex plane depends on φ_o. With small loss assumption ($Im[k_o] \lesssim 0$), if $0 < \varphi_o < \frac{\Phi}{2}$ ($\frac{\Phi}{2} < \varphi_o < \Phi$), α_o is located in the lower (upper) half α complex plane yielding unconventional plus (minus) unknowns $\bar{Y}_{i+}(\alpha)$ ($\bar{X}_{i-}(\alpha)$). The pole α_o can be captured by contour integration only if it is located in the proper sheet of α. This property is well illustrated in the w-plane: the pole α_o is associated to three different waves with same representation in α-plane but different in other complex planes such as η, m and w [36].

Using $\eta(w)$ (22) and $m(w)$ (23), we obtain that the incident wave, the face a reflected wave, the face b reflected wave show respectively the following poles in the w-plane

- for $0<\varphi_o<\frac{\Phi}{2}$: $w_o = -\varphi_o$, $w_{ao} = -2\Phi+\varphi_o$, $w_{bo} = -2\Phi-\varphi_o$
- for $\frac{\Phi}{2}<\varphi_o<\Phi$: $w_o^{(+\Phi)} = w_{ao}^{(+\Phi)} = -\varphi_o$, $w_{bo}^{(+\Phi)} = -2\Phi-\varphi_o$ and $w_o^{(-\Phi)} = w_{bo}^{(-\Phi)} = -2\Phi-\varphi_o$, $w_{ao}^{(-\Phi)} = -4\Phi+\varphi_o$

Note that the reader can extrapolate the following other cases using a similar procedure: $-\frac{\Phi}{2} < \varphi_o < 0$ and $-\Phi < \varphi_o < -\frac{\Phi}{2}$. Only some of the above poles are locate in the proper sheet ($-\Phi \le w \le 0$, see $\bar{w}$-plane properties in Appendix I of [36]) and they correspond to existing waves along the associated direction $\varphi = 0, +\Phi, -\Phi$.

Let us, now, suppose $0 < \varphi_o < \frac{\Phi}{2}$, the unconventional plus function $\bar{Y}_{i+}(\alpha)$ for $i = 1, 3, 5, 7$ can be decomposed in:

$$\bar{Y}_{i+}(\alpha) = \bar{Y}_{i+}^s(\alpha) + \frac{\bar{T}_{oi}}{\alpha-\alpha_o} \tag{78}$$

where $\bar{Y}_{i+}^s(\alpha)$ are standard plus functions representing the axial spectra without the GO components (in this case the incident wave). Since $0 < \varphi_o < \frac{\Phi}{2}$ only the GO pole w_o is located in the proper sheet ($-\Phi < w < 0$), therefore the incident wave is the only one that contributes to the residue $\bar{T}_{oi}$. According to (14) and the procedure described in [37] we define the source term:

$$\bar{n}_i(\alpha) = \frac{\bar{T}_{oi}}{\alpha-\alpha_o} \tag{79}$$

$\bar{T}_{oi}$ is the residue of $\bar{Y}_{i+}(\alpha)$ in α_o:

$$\bar{T}_{oi} = Res\left[\bar{Y}_{i+}(\alpha)\right]\Big|_{\alpha_o} = T_{oi}\left.\frac{d\alpha}{d\eta}\right|_{\eta_o} \tag{80}$$

with $T_{oi} = Res\left[Y_{i+}(\eta)\right]\big|_{\eta_o}$ and $\eta_o = -\tau_o\cos(w_o)$.

T_{oi} are obtained by using the Laplace transform of the GO field components along the $\varphi = 0$ direction in the η-plane. In this case the GO field is constituted by only the incident wave, see (77). Using Table I for definition of $\bar{Y}_{i+}(\alpha)$ in terms of longitudinal and tangential field components we obtain $\bar{T}_{oi}$ and $\bar{n}_i(\alpha)$.

On the contrary, if $\frac{\Phi}{2} < \varphi_o < \Phi$, only the pole $w_o^{(+\Phi)} = w_{ao}^{(+\Phi)}$ is located in the proper sheet $-\Phi < w < 0$. In this case the unconventional minus function $\bar{X}_{i-}(\alpha)$ for $i = 1, 3, 5, 7$ can be decomposed in:

$$\bar{X}_{i-}(\alpha) = \bar{X}^s_{i-}(\alpha) + \frac{\bar{U}_{oi}}{\alpha - \alpha_o} \tag{81}$$

where $\bar{X}^s_{i-}(\alpha)$ are standard minus functions representing the facial spectra without the GO components (in this case the incident wave and the face a reflected wave). $\bar{U}_{oi}$ is the residue of $\bar{X}^s_{i-}(\alpha)$ in α_o:

$$\bar{U}_{oi} = Res\left[\bar{X}_{i-}(\alpha)\right]\Big|_{\alpha_o} = U_{oi}\left.\frac{d\alpha}{dm}\right|_{m_o} \tag{82}$$

with $U_{oi} = Res\left[X_{i-}(m)\right]\big|_{m_o}$ and $m_o = m_{ao} = \tau_o\cos(-\varphi_o + \Phi)$.

In this second case, from (14), we define the source term:

$$\bar{n}_i(\alpha) = \frac{Res[\bar{X}_{(i)-}(\alpha) - \frac{\xi_-}{n_+}\bar{X}_{(i+1)-}(\alpha)]\Big|_{\alpha_o}}{\alpha - \alpha_o} \tag{83}$$

and therefore using (82):

$$\bar{n}_i(\alpha) = \frac{\bar{U}_{o(i)}}{(\alpha - \alpha_o)} + \frac{\tau_o + \alpha}{\sqrt{\tau_o^2 - \alpha^2}}\frac{\bar{U}_{o(i+1)}}{(\alpha - \alpha_o)} \tag{84}$$

Notice that, for $\frac{\Phi}{2} < \varphi_o < \Phi$, the $X_{-(i)}$ functions reported in (19) must be substituted with $X^s_{-(i)}$, which is the minus unknowns purified from the unconventional singular term via decomposition (in the Fredholm factorization the unknowns are always standard [37]).

$U_{o(i)}$ are obtained by using the Laplace transforms along the $\varphi = \pm\Phi$ directions in the $-m$ plane of the GO field components having singularities in the proper sheet of α (see Table I and (10)-(11)).

Let us focus the attention on the $\varphi = +\Phi$ case: the to-be-considered GO components are the incident wave and the face a reflected wave. These waves must be considered only if face a ($\varphi = +\Phi$) is not in shadow. Similar considerations hold for face b ($\varphi = -\Phi$) where we need to consider the incident wave and the face b reflected wave. Using Table I and (10)-(11) for definition of $\bar{X}_{i-}(\alpha)$ in terms of longitudinal and tangential field components we obtain $\bar{U}_{oi}$ and $\bar{n}_i(\alpha)$.

In the general case, the source term $\bar{n}_i(\alpha)$ assumes the following form

$$\bar{n}_i(\alpha) = \frac{If[\varphi_o < \frac{\Phi}{2}, \bar{T}_{o(i)}, \bar{U}_{o(i)} + \frac{\tau_o + \alpha}{\sqrt{\tau_o^2 - \alpha^2}}\bar{U}_{o(i+1)}]}{\alpha - \alpha_o} \tag{85}$$

where the explicit expressions of all non-zero $\bar{T}_{o(i)}$ and $\bar{U}_{o(i)}$ are reported in Table IV when the GO poles are related to the incident wave and the face a reflected wave ($0 < \varphi_o < \Phi$). Note that the signs of the residue terms in $\bar{n}_i(\alpha)$ are decided according to the orientation of the integration contour in the Fredholm factorization procedure, see [37] and section II-B.

TABLE IV
DEFINITIONS FOR THE SOURCE TERM $\bar{n}_i(\alpha)$ FOR $0 < \varphi_o < \Phi$.

$\bar{T}_{o1}$	$-j4E_o\frac{\pi}{\Phi}$
$\bar{T}_{o3}$	$j4E_o\frac{\pi}{\Phi}\sin(\frac{\pi\varphi_o}{2\Phi})$
$\bar{T}_{o5}$	$j4H_o\frac{\pi}{\Phi}$
$\bar{T}_{o7}$	$-j4H_o\frac{\pi}{\Phi}\sin(\frac{\pi\varphi_o}{2\Phi})$
$\bar{U}_{o1}$	$\frac{-2\pi j\left(E_o + E^{(a)}_{or}\right)}{\Phi}$
$\bar{U}_{o2}$	$\frac{-2\pi j\left(E_o - E^{(a)}_{or}\right)\cot(\frac{\pi\varphi_o}{2\Phi})}{\Phi}$
$\bar{U}_{o3}$	$\frac{2\pi j\left(E_o + E^{(a)}_{or}\right)\sin(\frac{\pi\varphi_o}{2\Phi})}{\Phi}$
$\bar{U}_{o4}$	$\frac{2\pi j\left(E_o - E^{(a)}_{or}\right)\cos(\frac{\pi\varphi_o}{2\Phi})}{\Phi}$
$\bar{U}_{o5}$	$\frac{2\pi j\left(H_o + H^{(a)}_{or}\right)}{\Phi}$
$\bar{U}_{o6}$	$-\frac{2\pi j\left(H_o - H^{(a)}_{or}\right)\cot(\frac{\pi\varphi_o}{2\Phi})}{\Phi}$
$\bar{U}_{o7}$	$-\frac{2\pi j\left(H_o + H^{(a)}_{or}\right)\sin(\frac{\pi\varphi_o}{2\Phi})}{\Phi}$
$\bar{U}_{o8}$	$\frac{2\pi j\left(H_o - H^{(a)}_{or}\right)\cos(\frac{\pi\varphi_o}{2\Phi})}{\Phi}$

$E^{(a)}_{or}$ and $H^{(a)}_{or}$ are cumbersome coefficients of the face a reflected wave available from GO. At normal incidence $E^{(a)}_{or}$ and $H^{(a)}_{or}$ are simple expressions:

$$\begin{aligned} E^{(a)}_{or} &= \Gamma^{\perp}_a E_o = \tfrac{Z_1\sin(\Phi-\varphi_o) - Z_o\sin(\Phi-\varphi_{ta})}{Z_1\sin(\Phi-\varphi_o) + Z_o\sin(\Phi-\varphi_{ta})}E_o \\ H^{(a)}_{or} &= \Gamma^{\parallel}_a E_o = \tfrac{Z_o\sin(\Phi-\varphi_o) - Z_1\sin(\Phi-\varphi_{ta})}{Z_o\sin(\Phi-\varphi_o) + Z_1\sin(\Phi-\varphi_{ta})}H_o \end{aligned} \tag{86}$$

with $\varphi_{ta} = \Phi + g(\Phi - \varphi_o)$, where $g(w)$ is defined in (49).

Note that the reader can extrapolate the case $-\Phi < \varphi_o < 0$ where we need to consider the reflected wave from face b.

Example

For the sake of readability, we present some explicit expressions of $\bar{n}_i(\alpha)$ when a dielectric wedge is illuminated by an E-polarized plane wave at normal incidence.

The first explicit expression under examination is $\bar{n}_1(\alpha)$ for $0 < \varphi_o < \frac{\Phi}{2}$ thus we need to evaluate $\bar{T}_{o1}$. In this case, the non-standard functions are the plus ones and the GO pole is $\eta_o = -\tau_o\cos(\varphi_o)$. Since $T_{oi} = Res\left[Y_{i+}(\eta)\right]\big|_{\eta_o}$, using Table II, we obtain that:

$$T_{o1} = 2\frac{\xi_+(\eta_o)}{n_+(\eta_o)}Res\left[V_{z+}(\eta, 0)\right]\big|_{\eta_o} \tag{87}$$

Since the GO component is only the incident wave, we can evaluate $Res\left[V_{z+}(\eta, 0)\right]\big|_{\eta_o} = jE_o$ using the η-Laplace transform for $\varphi = 0$

$$V^i_{z+}(\eta, 0) = \int_0^\infty E_o e^{jk_o\rho\cos(0-\varphi_o)}e^{j\eta\rho}d\rho = \frac{jE_o}{\eta - \eta_o} \tag{88}$$

Using (87) and (23) with $w_o = -\varphi_o$ we obtain

$$T_{o1} = -4jE_o\frac{\sin\varphi_o}{\sin\left(\frac{\pi}{\Phi}\varphi_o\right)} \tag{89}$$

We observe that since $\left.\frac{d\alpha}{d\eta}\right|_{\eta_o} = \frac{\pi}{\Phi}\frac{\sin\left(\frac{\pi}{\Phi}(-\varphi_o)\right)}{\sin(-\varphi_o)}$, $\bar{T}_{o1} = -4j\frac{\pi}{\Phi}E_o$ and the explicit expression of $\bar{n}_1(\alpha)$ results:

$$\bar{n}_1(\alpha) = \frac{-4j\frac{\pi}{\Phi}E_o}{\alpha - \alpha_o} \tag{90}$$

The second explicit expression under examination is $\bar{n}_1(\alpha)$ for $\frac{\Phi}{2} < \varphi_o < \Phi$ thus we need to evaluate $\bar{U}_{o1}$ and $\bar{U}_{o2}$. In this case, the non-standard functions are the minus ones and the GO pole present in the proper sheet of α-plane is $m_o^{(+\Phi)} = m_{ao}^{(+\Phi)} = \tau_o \cos(\Phi - \varphi_o)$ (incident and face a reflected wave of the facial spectra of face a). Since $U_{oi} = Res\left[X_{i-}(m)\right]|_{m_o}$, using Table II and (10)-(11), we obtain that:

$$U_{o1} = -\frac{\xi_-(m_o^{(+\Phi)})}{n_-(m_o^{(+\Phi)})} Res\left[s_{Vz+}(-m)\right]|_{m_o^{(+\Phi)}} \quad (91)$$

$$U_{o2} = \frac{k_o Z_o}{\xi_-^2(m_o^{(+\Phi)})} Res\left[d_{I\rho+}(-m)\right]|_{m_o^{(+\Phi)}} \quad (92)$$

We recall from the previous subsection that only the facial spectra of face a have singularities in the proper sheet of α plane, therefore we obtain that:

$$Res\left[s_{Vz+}(-m)\right]|_{m_o^{(+\Phi)}} = Res\left[V_{z+}(-m,+\Phi)\right]|_{m_o^{(+\Phi)}} \quad (93)$$
$$Res\left[d_{I\rho+}(-m)\right]|_{m_o^{(+\Phi)}} = Res\left[I_{\rho+}(-m,+\Phi)\right]|_{m_o^{(+\Phi)}} \quad (94)$$

Without loss of generality let us focus the attention on U_{o1}. Since the GO components are the incident and the face a reflected waves we can evaluate $Res\left[V_{z+}(-m,+\Phi)\right]|_{m_o^{(+\Phi)}}$ using the $-m$ Laplace transform for $\varphi = +\Phi$

$$V_{z+}^g(-m,\Phi) = \int_0^\infty (E_o + E_{or}^{(a)}) e^{jk_o\rho\cos(\Phi-\varphi_o)} e^{-jm\rho} d\rho \quad (95)$$

thus, using (86), $V_{z+}^g(-m,\Phi) = \frac{-jE_o(1+\Gamma_a^\perp)}{m-m_o^{(+\Phi)}}$.

The evaluation of the quantities U_{oi} and $\bar{U}_{oi}$ can be easily carried out using the w-plane together with the m-plane. We recall that $m_o^{(+\Phi)}$ corresponds to $w_o^{(+\Phi)} = -\varphi_o$. Using (23) we obtain:

$$U_{o1} = -j2E_o(1+\Gamma_a^\perp)\frac{\sin(\Phi-\varphi_o)}{\sin(\frac{\pi}{\Phi}\varphi_o)} \quad (96)$$

We observe that since $\frac{d\alpha}{dm}\big|_{m_o^{(+\Phi)}} = \frac{\pi}{\Phi}\frac{\sin\frac{\pi\varphi_o}{\Phi}}{\sin(\Phi-\varphi_o)}$ we obtain

$$\bar{U}_{o1} = -2j\frac{\pi}{\Phi}E_o(1+\Gamma_a^\perp) \quad (97)$$

and following the same procedure, we can evaluate the explicit expression of $\bar{U}_{o2}$:

$$\bar{U}_{o2} = -2j\frac{\pi}{\Phi}E_o(1-\Gamma_a^\perp)\cot(\frac{\pi\varphi_o}{2\Phi}) \quad (98)$$

In this case, the source term $\bar{n}_1(\alpha)$ results:

$$\bar{n}_1(\alpha) = \frac{-j2\frac{\pi}{\Phi}E_o}{\alpha-\alpha_o}\left[(1+\Gamma_a^\perp) + \frac{k_o+\alpha}{\sqrt{k_o^2-\alpha^2}}(1-\Gamma_a^\perp)\cot(\frac{\pi\varphi_o}{2\Phi})\right] \quad (99)$$

APPENDIX II
THE g AND g_1 FUNCTIONS

The functions $g(w)$ and $g_1(w_1)$, see (49) and (50), are multi-valued functions [42] used extensively throughout the paper, for example in the recursive equations (53). $g(w)$ and $g_1(w_1)$ show branch points located respectively in $\pm w_b + n\pi$ and $\pm w_{1b} + n\pi$ with $n \in \mathbb{N}$, $w_b = -j\,\mathrm{arccosh}\sqrt{\varepsilon_r}$ and $w_{1b} = -\arccos(1/\sqrt{\varepsilon_r})$. We assume vertical branch cuts, *i.e.* the line $(\pm w_b, \pm j\infty)$ for the branch point $\pm w_b$ and the line $(\pm w_{1b}, \pm j\infty)$ for the branch point $\pm w_{1b}$. We remark that our branch choice is different from the one done by Budaev [18].

We assert that the Snell law in the spectral domain (22) ensures the continuity relation:

$$\hat{F}_+(w,\pm\Phi) = \hat{F}_+(w_1,\pm\Phi_1) \quad (100)$$

This property is used in the procedure to derive the recursive equations (53). Let us focus the attention on the properties of $g(w)$ and $g_1(w_1)$ in the recursive equations (53) for the estimation of the GTD diffraction coefficient (76). As discussed in subsections IV-A and IV-B, we require the evaluation of the axial spectra $\varphi = 0$ and $\varphi = \pi$ respectively in the interval $-\pi - \Phi < w < -\pi + \Phi$ and $-\pi_1 - \Phi < w_1 < -\pi + \Phi_1$.

We recall that the recursive equations (53) are substantially of these two kinds:

$$\hat{F}(w) = \Theta[\hat{F}(w+2\Phi), \hat{F}_\pi(\Phi_1 + g(w+\Phi))] \quad (101)$$

$$\hat{F}_\pi(w_1) = \Theta_\pi[\hat{F}(\Phi + g_1(w_1+\Phi_1)), \hat{F}_\pi(w_1+\Phi_1)] \quad (102)$$

We observe that for each real w, (101) requires the evaluation of $\hat{F}(w)$ and $\hat{F}_\pi(w_1)$ with real arguments w and w_1. On the contrary, for each real w_1, (102) requires the evaluation of $\hat{F}_\pi(w_1)$ with real arguments w_1 and the evaluation of $\hat{F}(w)$ with complex arguments w determined by the mapping:

$$w = \Phi + g_1(w_1 + \Phi_1) \quad (103)$$

Fig. 17 shows (103) for $\varepsilon_r = 3 - j0.1$ and for different values of Φ in the interval $-\pi - \Phi_1 < w_1 < -\Phi_1$ highlighting the cardinal points: $w_1 = -\Phi_1$, $w_1 = -\pi + \Phi_1$, $w_1 = -\pi - \Phi_1$.

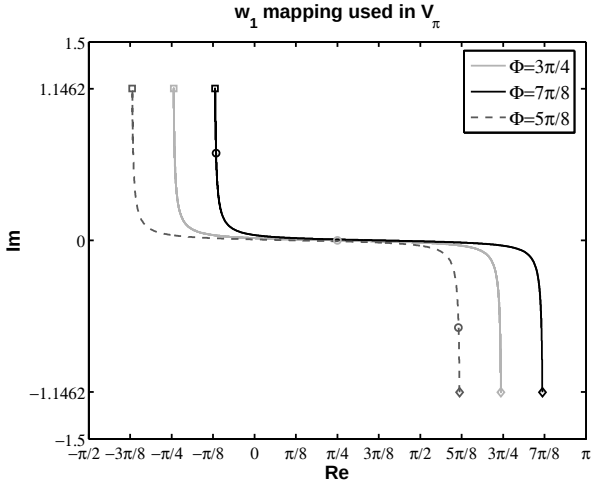

Fig. 17. $w = \Phi + g_1(w_1 + \Phi_1)$ mapping for $\varepsilon_r = 3 - j0.1$ and for different values of Φ in the interval $-\pi - \Phi_1 < w_1 < -\Phi_1$. The map starts from $w_1 = -\Phi_1$ that yields $w = \Phi - \arccos(\sqrt{\varepsilon_r})$ and goes all over the gray lines as long as $w_1 = -\pi - \Phi_1$ is mapped into $w = -\Phi_1 + \arccos(\sqrt{\varepsilon_r})$. The symbols $\diamondsuit, \bigcirc, \square$ respectively are the mapped value for $w_1 = -\Phi_1, -\pi + \Phi_1, -\pi - \Phi_1$.

APPENDIX III
THE OUTER AXIAL STARTING SPECTRA

With the assumption of no losses, we notice that using complex conjugation of (39) and substituting $-u$ to u we obtain the same equations with changed in sign sources, *i.e.* $-n_{1,3}(u)$ (see Appendix I). It yields $P_i(u) = -P_i^*(-u)$.

Using the w-plane in $M(u,u')$, *i.e.* $M(-j(\frac{\pi}{\Phi}w + \frac{\pi}{2}), u')$, we observe that for real u' and w:

$$M(-j(\frac{\pi}{\Phi}w + \frac{\pi}{2}), u') = -M^*(-j(\frac{\pi}{\Phi}w + \frac{\pi}{2}), -u') \quad (104)$$

These properties yield a real sum for $-\Phi \leq w \leq 0$ in (43),(45)

$$\sum_{i=-\frac{A}{h}}^{\frac{A}{h}} M\left[-j(\frac{\pi w}{\Phi}+\frac{\pi}{2}), hi\right] P_{2,4}(hi) \tag{105}$$

and since $n_{1,3}(u)$ are purely imaginary for $w \epsilon \mathbb{R}$, we obtain purely imaginary outer spectra $\{\hat{V}_+(w), \hat{I}_+(w)\}$for $-\Phi \leq w \leq 0$.

REFERENCES

[1] J. Radlow, "Diffraction by a right-angled dielectric wedge," *Intern. J. Enging Sci.*, vol. 2, n.3, pp. 275-290, Jun. 1964

[2] Y.Yu. Zavadskii, "Certain diffraction problems in contiguous liquid and elastic wedges," *Soviet Physics-Acoustics.*, vol. 12, pp. 170-179, 1966.

[3] E.A. Kraut, and G.W. Lehaman, "Diffraction of electromagnetic waves by a right-angled dielectric wedge," *J. Math. Phys.*, vol. 10, pp. 1340-1348, 1969.

[4] E. N. Vasil'ev, and V.V. Solodukhov, "Diffraction of electromagnetic waves by a dielectric wedge," *Radiophysics and Quantum Electronics*, vol. 17, pp. 1161-1169, 1974.

[5] A.A. Aleksandrova, and N.A. Khiznyak, "Diffraction of Electromagnetics Waves by a Dielcctric Wedge," *Sov. Phys. Tech. Phys.*, vol. 19, pp. 1385-1389, May 1975.

[6] T.K. Wu, and L.L. Tsai., "Scattering by a Dielectric Wedge: A numerical Solution," *IEEE Trans. Antennas Propagat.*, vol. 25, pp. 570-571, 1977.

[7] L. Lewin, and I. Sreenivasiah, Diffraction by a dielectric wedge, Rep. No.47, Dept Electr. Engin., Univ. of Colorado, Boulder, CO, USA, 1979.

[8] A.D. Rawlins, "Diffraction by a dielectric wedge,"*J. Inst. Math. Appl.*, vol. 19, pp. 231-279, 1977.

[9] A.D. Rawlins, "Diffraction by, or diffusion into, a penetrable wedge," *Proceedings Royal Society. Mathematical, Physical and Engineering Sciences.*, vol. 455, pp. 2655- 2686, 1999.

[10] S. Berntsen, "Diffraction of an electric polarized wave by a dielectric wedge.," *SIAM J. Appl. Math.*, vol. 43, pp. 186-211, 1983.

[11] R.H.T. Bates, "Toward an algorithm for dielectric -edge diffraction coefficients," *IEE Proceedings*, vol.132, Pt. H. 7, pp. 461-467, 1985.

[12] S.Y. Kim, J.W. Ra, and S.Y. Shin, "Diffraction by an arbitrary -angled dielectric wedge: Part I - Physical optics," *IEEE Trans. Antennas Propagat.*, vol. 39, n. 9, pp. 1272-1281, Sept. 1991.

[13] S.Y. Kim, J.W. Ra, and S.Y. Shin, "Diffraction by an arbitrary -angled dielectric wedge: Part II - Correction to Physical Optics Solution," *IEEE Trans. Antennas Propagat.*, vol. 39, n. 9, pp. 1282-1292, Sept. 1991.

[14] E. Marx, "Electromagnetic scattering from a dielectric wedge and the single hypersingular integral equation," *IEEE Trans. Antennas Propagat.*, vol. 41, pp. 1001-1008, 1993.

[15] A.V. Osipov, "On the method of Kontorovich-Lebedev integrals in problems of wave diffraction in sectorial media," in *Problems of diffraction and propagation of waves*, Vol. 25, pp. 173-219, St Petersburg University Publications, 1993.

[16] K. Fujii, "RayleighWave scattering at various corners: Investigation in the wider range of wedge angles," *Bull. Seism. Soc. Am.*, vol. 84, pp. 1916-1924, 1994.

[17] G.L. Wojcik, "A formulation of self-similar dielectric wedge diffraction," Proc. IEEE Antennas and Propagat. Int. Symp, pp.1068-1071, 1995.

[18] B. Budaev, *Diffraction by wedges*, London, UK: Longman Scient., 1995.

[19] T.B.A. Senior, and J.L. Volakis, *Approximate boundary conditions in electromagnetics*, London, UK: IEE, 1995.

[20] G. Stratis, V. Anantha, and A. Taflove, "Numerical Calculation of Diffraction Coefficients of Generic Conducting and Dielectric Wedges using FDTD," *IEEE Trans. Antennas Propagat.*, vol. 45, pp. 1525-1529, 1997.

[21] J.P. Croisille, and G. Lebeau, *Diffraction by an immersed elastic wedge*, Lecture notes in math. 1723, Berlin, Germany: Springer-Verlag, 1999.

[22] V.V. Kamotski, L.Ju. Fradkin, B.A. Samokish, V.A. Borovikov, V.M. Babich, "On Budaev and Bogys approach to diffraction by a 2D traction-free elastic wedge," *SIAM J.Appl. Math.*, vol. 67, n.1, pp. 235-259, 2006.

[23] V.S. Buldyrev, and M.A. Lyalinov, *Mathematical Methods in Modern Diffraction Theory*, Tokio, Japan: Science House Inc., 2001.

[24] A.K. Gautesen, "Scattering of a Rayleigh wave by an elastic wedge whose angle is greater than 180 degrees," *ASME J. Appl. Mech.*, vol. 68, pp. 476-479, 2001.

[25] A.S. Starkov, "Diffraction by dielectric wedge," in Proc. of Days on Diffraction Internat. Seminar, St.Petersburg, Russia, May 2001, pp. 256-266.

[26] V.G. Daniele, R.D. Graglia, "Approximate Diffraction coefficients for the right-angled penetrable wedges," in Proceedings of 2001 International Conference on Electromagnetics in Advanced Applications (ICEAA01), Torino, Italy, Sept. 2001, pp. 407-411.

[27] A.G. Tyzhnenko, "Cylindrical E-wave Scattering by a right angle dielectric wedge," *Electromagnetics*, vol. 22, pp. 487-497, 2002.

[28] V.G. Daniele, "The Wiener-Hopf technique for penetrable wedge problems," in Proc. of URSI General Assembly, New Delhi, India, Oct. 2005.

[29] M.A. Salem, A. Kamel, and A.V. Osipov, "Electromagnetic fields in the presence of an infinite dielectric wedge," *Proceedings of Royal Society: Mathematical, Physical and Engineering Sciences*, vol. 462, pp. 2503-2522, 2006.

[30] S.Y. Kim, "Hidden Rays of diffraction for dielectric wedge," *Radio Science*, vol. 42: RS6S07, 2007.

[31] J.D. Morgan, and A.D. Rawlins, "An iterative approach to scattering by edges and wedges," *Wave Motion*, vol. 44, pp. 176-204, 2007.

[32] V.M. Babich, M.A. Lyalinov, and V.E. Grikurov, *Sommerfeld-Malyuzhinets Technique in Diffraction Theory*, Oxford, UK: Alpha Science, 2007.

[33] V. Daniele, "The Wiener-Hopf technique for impenetrable wedges having arbitrary aperture angle," *SIAM Journal of Applied Mathematics*, vol.63, n.4, pp.1442-1460, 2003.

[34] V. Daniele, *An introduction to the Wiener-Hopf Technique for the solution of electromagnetic problems*, Internal Report ELT-2004-1, Dipartimento di Elettronica, Politecnico di Torino, Sep. 2004, http://personal.delen.polito.it/vito.daniele/.

[35] V.G. Daniele and G. Lombardi, "The Wiener-Hopf technique for impenetrable wedge problems," in Proc. of Days on Diffraction Internat. Conf., invited paper, pp. 50-61, Saint Petersburg, Russia, June 2005, doi: 10.1109/DD.2005.204879.

[36] V. Daniele, and G. Lombardi, "Wiener-Hopf Solution for Impenetrable Wedges at Skew Incidence," *IEEE Trans. Antennas Propagat.*, vol. 54, n. 9, pp. 2472-2485, Sept. 2006, doi: 10.1109/TAP.2006.880723.

[37] V.G. Daniele, and G. Lombardi, "Fredholm Factorization of Wiener-Hopf scalar and matrix kernels," *Radio Science*, vol. 42: RS6S01, 2007, doi:10.1029/2007RS003673.

[38] N.P. Vekua, *Systems of Singular Integral Equations*, Groningen, The Netherlands: Noordhoff, 1967.

[39] V. Daniele, and G. Lombardi, "The Wiener-Hopf method applied to dielectric angular regions: The wedge," in Proc. of Int. Conf. on Electromagnetics in Advanced Applications (ICEAA09), Torino, Italy, Sept. 2009, pp. 489-492, doi: 10.1109/ICEAA.2009.5297388.

[40] V. Daniele, and G. Lombardi, "The Wiener-Hopf method applied to multiple angular region problems: The penetrable wedge case," in Proc. of IEEE Antennas and Propagation Society Int. Symp., Jun. 2009, Charleston, SC, pp. 1-4, doi: 10.1109/APS.2009.5172090.

[41] V.G. Daniele, "The Wiener-Hopf Formulation of the Penetrable Wedge Problem: Part I," *Electromagnetics*, Vol.30, n.8, pp.625643, 2010.

[42] V.G. Daniele, "The Wiener-Hopf Formulation of the Penetrable Wedge Problem: Part II," submitted to Electromagnetics.

[43] L.V. Kantorovich and V.I. Krylov, *Approximate methods of higher analysis*, Groningen, The Netherlands: Noordhoff, 1964.

[44] V.G. Daniele, "Rotating Waves in the Laplace Domain for Angular Regions," *Electromagnetics*,, vol. 23, n. 3, pp. 223-236, 2003.

[45] R. G. Kouyoumjian and P. H. Pathak, "A uniform geometrical theory of diffraction for an edge in a perfectly conducting surface," *Proc. IEEE*, vol. 62, pp. 1448-1461, Nov. 1974.

[46] R. Tiberio, G. Pelosi, G. Manara, and P. H. Pathak, "High-frequency scattering from a wedge with impedance faces illuminated by a line source, Part I: Diffraction," *IEEE Trans. Antennas Propagat.*, vol. 37, pp. 212-218, Feb. 1989.

[47] R.G. Kouyoumjian, G. Manara, P. Nepa and B.J.E. Taute, "The diffraction of an inhomogeneous plane wave by a wedge," *Radio Science*, vol. 31, n. 6, pp. 1387-1397, Nov.-Dec. 1996.

[48] G. Manara, R. Tiberio, G. Pelosi, and P. H. Pathak, "High-frequency scattering from a wedge with impedance faces illuminated by a line source, Part II: Surface waves," *IEEE Trans. Antennas Propagat.*, vol. 41, pp. 877-883, July 1993.